

Therapeutic benefits of maintaining mitochondrial integrity and calcium homeostasis by forced expression of Hsp27 in chemotherapy-induced peripheral neuropathy



Virendra Bhagawan Chine^{a,1}, Ngan Pan Bennett Au^{a,1}, Chi Him Eddie Ma^{a,b,c,*}

^a Department of Biomedical Sciences, City University of Hong Kong, Tat Chee Avenue, Hong Kong

^b Centre for Biosystems, Neuroscience, and Nanotechnology, City University of Hong Kong, Tat Chee Avenue, Hong Kong

^c State Key Laboratory in Marine Pollution, City University of Hong Kong, Tat Chee Avenue, Hong Kong

ARTICLE INFO

Keywords:

Chemotherapy-induced peripheral neuropathy
Heat shock protein 27
Vincristine
Mechanical and cold allodynia
Axon degeneration
Demyelination
Intracellular calcium

ABSTRACT

Background: Vincristine, a widely used antineoplastic agent, is known to be neurotoxic and to lead to chemotherapy-induced peripheral neuropathy (CIPN), which is characterized by nerve damage. Growing evidence suggests that disruption of intracellular calcium homeostasis in peripheral neurons contributes largely to the pathological conditions of CIPN. Our previous study showed that forced expression of a peripheral nerve injury-induced small heat shock protein (Hsp), Hsp27, accelerates axon regeneration and functional recovery. In the current study, we examined whether neuronal expression of human Hsp27 (hHsp27) can prevent the inhibitory effects of vincristine in two mouse models of peripheral nerve injury, namely, sciatic nerve crush and CIPN.

Methods: The protective effects of hHsp27 against vincristine were examined in mouse models of both sciatic nerve crush and CIPN using multiple approaches, including animal behavioral tests, histology, electrophysiology, transmission electron microscopy and calcium imaging.

Results: Vincristine delayed functional recovery in littermate mice; however, hHsp27 Tg mice were unaffected after vincristine treatment and sciatic nerve crush. In CIPN mice, hHsp27 protected against vincristine-induced mechanical and cold allodynia by preventing axonal degeneration, demyelination, mitochondrial dysfunction, and apoptosis. Strikingly, vincristine-induced calcium influx was markedly attenuated in sensory neurons of hHsp27 Tg mice.

Conclusions: Our findings suggest that preserving myelin and mitochondrial integrity as well as maintaining intracellular calcium homeostasis is beneficial for preventing CIPN, and these findings shed new light on the development of anti-CIPN drugs.

1. Introduction

Cancer chemotherapy refers to the use of pharmacological agents to control the growth and proliferation of malignant cells. Paradoxically, chemotherapeutic agents that mainly target proliferating cancer cells also have potent off-target effects on healthy neurons, a pathological condition known as chemotherapy-induced peripheral neuropathy (CIPN) (Au et al., 2014; Jaggi and Singh, 2012). Due to the absence of an effective blood-nerve barrier in the peripheral nervous system (PNS), sensory neurons and nerves are more susceptible to damage by anti-neoplastic drugs than those in the central nervous system (CNS), which is usually well protected by the blood-brain barrier (Starobova and Vetter, 2017). CIPN is a predominantly sensory neuropathy that may be

accompanied by motor disturbance. There is accumulating evidence to suggest that CIPN pathogenesis is related to the development of axonopathy (axon degeneration) and neuropathy (neuronal cell death) as well as dysfunctions in mitochondria and calcium channels (Berbusse et al., 2016; Canta et al., 2015; Cashman and Hoke, 2015; Fukuda et al., 2017; Siau and Bennett, 2006), although the underlying pathophysiology remains unclear. A recent meta-analysis study on the prevalence of CIPN found that as many as 68% of cancer patients receiving chemotherapy develop CIPN, and approximately 30% of patients still experience CIPN 6 months or longer after stopping chemotherapy (Seretny et al., 2014). CIPN remains a major reason that cancer patients withdraw from lifesaving treatments. Currently, there are no effective or preventive treatments for CIPN.

* Corresponding author at: Department of Biomedical Sciences, City University of Hong Kong, Tat Chee Avenue, Hong Kong.
E-mail address: eddiema@cityu.edu.hk (C.H.E. Ma).

¹ These authors contributed equally to this work.

Vincristine is an antimitotic vinca alkaloid that is widely used to treat several types of malignancies, such as leukemia, lymphomas, Hodgkin's disease, sarcoma, neuroblastoma, and small cell carcinoma (Staff et al., 2017; Windebank and Grisold, 2008). While vincristine has potent antineoplastic activity, however, approximately 80% of the patients treated with vincristine experience severe sensorimotor neuropathy (Deangelis et al., 1991; Haim et al., 1994; Lavoie Smith et al., 2015), including numbness and tingling in the upper and lower limbs, loss of tendon reflexes, muscle cramping and weakness in distal muscles (Jaggi and Singh, 2012; Quasthoff and Hartung, 2002; Windebank and Grisold, 2008). In some cases, CIPN can persist for months or even years after completion of vincristine treatment (Gottschalk et al., 1968; Rosenthal and Kaufman, 1974). CIPN leads to the irreversible loss of sensory and motor functions, which greatly affects patients' ability to perform daily activities and quality of life. Vincristine binds to β -tubulin (the building block of the cytoskeleton in cells and axons) to exert its antineoplastic effects by inhibiting microtubule dynamics in the mitotic spindle, resulting in cell cycle arrest and inhibition of cell division in proliferating cancer cells (Jordan et al., 1991; Jordan and Wilson, 2004). However, due to its ability to cross the blood-nerve barrier, vincristine can also bind to β -tubulin to exert off-target effects on peripheral sensory neurons (Windebank and Grisold, 2008). Our previous study demonstrated that vincristine disrupts neuronal cytoskeletal architecture, which results in neurite outgrowth inhibition in cultured dorsal root ganglion (DRG) neurons, by promoting microtubule depolymerization in a similar way as in cancer cells (Au et al., 2014). Studies in animal models and patients implicate axonal degeneration, loss of intraepidermal nerve fibers (IENFs), demyelination, neuronal apoptosis, mitochondria dysfunction and reduction of sensory nerve action potential (SNAP) as common processes in CIPN pathology (Boehmerle et al., 2014; Canta et al., 2015; Chan et al., 1980; Chaudhry et al., 1994; Han and Smith, 2013; Kroigard et al., 2014; Liu et al., 2017; Park et al., 2013; Periquet et al., 1999; Starobova and Vetter, 2017).

Intracellular calcium ions act as universal second messengers for a wide range of important physiological processes, including neurotransmission, neuronal excitability, enzymatic activity and transcriptional regulation (Berridge et al., 2000). Calcium homeostasis is tightly regulated in neurons by several signaling pathways involving extracellular calcium uptake, intracellular calcium release and mitochondrial calcium uptake (Berridge, 1998; Brini et al., 2014). Growing evidence suggests that altered calcium homeostasis in peripheral neurons may contribute to the pathological conditions of CIPN (Starobova and Vetter, 2017). For instance, two platinum-based compounds, oxaliplatin and cisplatin, affect calcium signaling pathways, alter mitochondrial function and activate apoptosis pathways, leading to neuronal cell death (Carozzi et al., 2015; Dasari and Tchounwou, 2014; Meijer et al., 1999). Oxalate, a known metabolite of oxaliplatin and calcium chelator, has been suggested to contribute to the development of oxaliplatin-induced peripheral neuropathy. Local administration of oxalate into the hindlimb of mice induces mechanical allodynia, likely as a consequence of chelation of extracellular calcium ions (Deuis et al., 2013). In DRG neurons, cisplatin upregulates the expression and current of N-type voltage-gated calcium channels (VGCCs). Increases in VGCC currents and protein expression have been linked to the development of neuropathic pain (Snutch, 2005; Vanegas and Schaible, 2000; Vink and Alewood, 2012; Zamponi et al., 2009). Another commonly used antineoplastic drug, paclitaxel, which inhibits the cancer cell cycle, causes rapid mitochondrial depolarization and calcium release via the mitochondrial permeability transition pore (mPTP) (Kidd et al., 2002; Mironov et al., 2005). Paclitaxel also induces oscillatory changes in cytosolic calcium levels in a human neuronal cell line (Boehmerle et al., 2006). All of these studies suggest that disruption of cytoskeletal integrity, neuronal survival and dysregulation of calcium homeostasis could be the major underlying causes of CIPN.

Injuring the peripheral axons of DRG neurons initiates hundreds of

transcriptional changes, resulting in vast alterations in protein composition (Costigan et al., 2002; Griffin et al., 2007). Expression profile studies have revealed that a small heat shock protein (Hsp), Hsp27, is highly upregulated after peripheral nerve injury (Costigan et al., 1998). Hsp27 is a chaperone protein that acts to protect cells from insults such as heat stress, oxidative stress and ischemia (Benn et al., 2002; Huot et al., 1996; Lavoie et al., 1993). Hsp27 facilitates the refolding of misfolded proteins into active conformations to maintain protein homeostasis because stress results in protein misfolding and aggregation. It is therefore not surprising that Hsp27 is implicated in the pathologies of protein misfolding diseases that are associated with abnormal protein aggregation, such as Alzheimer's disease and Parkinson's disease (Muchowski, 2002; Pichon et al., 2004; Wilhelms et al., 2006), and is regarded as a potential therapeutic target. Hsp27 also functions as an actin-capping protein that plays an important role in actin polymerization and stabilization (Benndorf et al., 1994; Chaudhuri and Smith, 2008; Pichon et al., 2004). Hsp27 is the Hsp that is induced the most after peripheral nerve injury, whilst the expression levels of other Hsp family members remain unchanged (Costigan et al., 1998). Hsp27 protects somatosensory and motor neurons from axonal injury by preventing apoptosis (Benn et al., 2002; Costigan et al., 1998). Our previous studies demonstrated that the upregulation of Hsp27 markedly enhances the intrinsic regenerative capacity of adult sensory neurons, accelerates axon regeneration and functional recovery (Ma et al., 2011b), and protects sensory neurons from terminal axonal atrophy in a mouse model of diabetic neuropathy (Kornegut et al., 2012).

Vincristine is known to inhibit axonal growth in DRG neurons after peripheral nerve injury (Pan et al., 2003). Our recent study demonstrated the adverse effect of vincristine on microtubule organization and the cellular mechanical properties of adult DRG neurons in mice (Au et al., 2014). In the current study, we tested the neuroprotective effects of hHsp27 forced expression in a mouse model of CIPN. We first demonstrated that primary DRG neurons prepared from hHsp27 transgenic (Tg) mice overcame vincristine-induced neurite outgrowth inhibition in vitro, and accelerated in vivo sensory and motor functional recovery following sciatic nerve crush injury. In a mouse model of CIPN, forced expression of hHsp27 prevented the development of mechanical and cold allodynia, axonal degeneration of IENFs, mitochondrial dysfunction, neuronal apoptosis and aberrant calcium influx into adult sensory neurons. Our results clearly demonstrated that forced expression of hHsp27 completely prevented the development of vincristine-induced CIPN symptoms in mice via multiple mechanistic pathways.

2. Materials and methods

2.1. Animals

All animal experiments and euthanasia were performed in compliance with guidelines from the Institutional Animal Care and Use Committee (IACUC) and with approval of the Animal Research Ethics Sub-Committee at City University of Hong Kong and Department of Health, HKSAR. Adult male hHsp27 Tg and their age-matched wild-type (WT) littermates (LM) (8–12 weeks old) were used in all experiments. The generation of hHsp27 Tg mice was described in detail previously (Ma et al., 2011b). Briefly, the coding sequence of hHsp27 was first subcloned into the *Xba*I site of a Thy1.2 expression cassette (Caroni, 1997), linearized using *Eco*RI and *Pvu*I restriction enzymes, and microinjected into fertilized B6C3F1 mouse oocytes for the generation of hHsp27 Tg mice. The mice were genotyped by PCR amplification of genomic DNA as described (Ma et al., 2011b). The hHsp27 transgene was expressed postnatally under the control of a neuronal-specific Thy1.2 promoter to ensure that the embryonic development of the nervous system remained unaffected in hHsp27 Tg mice (Kornegut et al., 2012; Ma et al., 2011a). The hHsp27 Tg mice were backcrossed with WT C57BL/6 mice, a commonly used mouse strain in CIPN animal

model studies, to ensure that the data generated from the current study are comparable to those from other CIPN studies. The mice were housed randomly in groups of 5–6 animals per cage with free access to food and water and maintained on a 12:12-h light/dark cycle.

2.2. Primary dissociated DRG cultures

Adult hHsp27 Tg and their age-matched LM mice (8–12 weeks old) were used for primary cultures of dissociated DRG neurons, as described (Au et al., 2014; Au et al., 2016; Ma et al., 2011b). Briefly, DRGs were digested with collagenase/dispase II (Roche Diagnostics), trypsinized and mechanically dissociated using flame-polished Pasteur pipettes of three different diameters. Two thousand DRG neurons were plated in an 8-well chamber (Millipore) precoated with poly-D-lysine and laminin (Sigma Aldrich) and cultured in Neurobasal (NB) medium supplemented with 2 ng/ml GDNF (Sigma Aldrich), 50 ng/ml NGF, B27, 200 mM L-glutamine, penicillin/streptomycin (Gibco), and 10 μM Ara-C (Sigma Aldrich). Vincristine was first diluted in NB medium and applied to the cultures at final concentrations of 0.5, 2.5 and 10 ng/ml 1 h after plating. DRG neurons were cultured for 17 h, followed by a neurite outgrowth assay.

2.3. Neurite outgrowth and cell survival assays

DRG neurons were fixed with 4% paraformaldehyde (PFA), blocked with 0.5% bovine serum albumin (BSA)/0.1% Triton X-100 (Sigma Aldrich), and incubated with anti-βIII-tubulin primary antibodies (Sigma Aldrich), followed by Alexa Fluor 488-conjugated secondary antibodies (Molecular Probes) for the neurite outgrowth assay and cell survival analysis.

For the neurite outgrowth assay, nonoverlapping images were photographed with a 10× objective using a Nikon Eclipse 90i epifluorescence microscope with a motorized stage. The total neurite length of each DRG neuron was measured automatically using WIS-NeuroMath software (Weizmann Institute of Science) (Au et al., 2014; Au et al., 2016; Ma et al., 2011b). The mean total neurite length was calculated from at least 250 DRG neurons. The data are representative of three independent experiments, and the measurements were repeated in duplicate. βIII-tubulin-positive neurons with a fluorescence intensity over 170 arbitrary units (A.U.) and intact neurites adjacent to the cell bodies were counted as healthy neurons for the neurite outgrowth and survival assays.

2.4. Vincristine administration

Vincristine was diluted in saline at a final concentration of 0.05 mg/ml, and the mice were injected intraperitoneally (i.p.) in two 5-day cycles with a 2-day break between cycles. For instance, each mouse received ten i.p. injections of vincristine (0.05 mg/kg) or 0.9% saline as the vehicle control on days 0–4 and 7–11 (Flatters and Bennett, 2004; Siau and Bennett, 2006; Siau et al., 2006) (see Figs. 2A and 3A for detailed experimental paradigm) ($n = 11$ –12 per genotype). The mice developed mechanical and cold allodynia within 2 weeks after the first injection of vincristine (Flatters and Bennett, 2004; Siau and Bennett, 2006) and exhibited an extensive loss of IENFs (Siau et al., 2006).

2.5. Sciatic nerve crush

On day 12 (i.e., 1 day after the last vincristine administration), sciatic nerve crush was performed at the level of the external rotator muscles, just distal to the sciatic notch, on anesthetized vincristine- or saline-treated mice (Asthana et al., 2018; Au et al., 2016; Ma et al., 2011a; Ma et al., 2011b). The left sciatic nerve was crushed with smooth forceps (Fine Science Tools) for 15 s. After crush injury, the overlying muscle and skin were sutured using 5–0 sutures (Ethilon), and the animals were allowed to recover on a heating pad. The surgeon

was blinded to the genotypes and treatments.

2.6. Animal behavioral assessments

All animal behavioral assessments were performed in a quiet, temperature- and humidity-controlled room from 10 a.m. to 3 p.m., and only male mice were used. The observers were blinded to the genotypes and treatments. Baseline recordings were taken on day 0 before the first vincristine injection. For functional recovery assessment after sciatic nerve crush, we performed tests of sensory (pinprick assay) and motor functional recovery (toe spreading and grip strength tests) on day 12 after the first vincristine i.p. injection (see Fig. 2A for detailed experimental paradigm). To assess CIPN symptoms, including mechanical and cold allodynia, we performed electronic von Frey filament and acetone drop tests after the first i.p. injection of vincristine (see Fig. 3A for the detailed experimental paradigm). We first assessed the left hindpaw and then assessed the right hindpaw of the same animal at least 1 h after the left hindpaw assessment since vincristine is known to induce bilateral peripheral neuropathy (Siau and Bennett, 2006).

2.6.1. Pinprick sensory assay

Pinprick assay was used to assess sensory functional recovery after sciatic nerve crush injury (Au et al., 2016; Ma et al., 2011b). The mice were first habituated to wire mesh cages for 30 min. After habituation, an insect pin (size 000; Fine Science Tools) was gently applied to the lateral plantar surface (representing the sensory field of the sciatic nerve) of the ipsilateral hindpaw. The plantar surface was divided into 5 different areas, and pinprick stimulation was applied twice from the most lateral toe (i.e., score = 5) to the heel (i.e., score = 1). The mice were scored for a particular area if a brisk withdrawal response was observed upon pinprick stimulation. The mice scored 0 if a withdrawal response was not elicited in these five areas.

2.6.2. Toe spreading test

Motor functional recovery was assessed using a toe spreading motor assay (Au et al., 2016; Ma et al., 2011b). The mice were covered using a piece of thin cotton towel and lifted up by their tails, clearly exposing their hindpaws for assessment. The toe spreading reflex was scored as follows: 0 for no clear spreading of the toes, 1 for intermediate spreading of the toes that was not sustained for 2 s, and 2 for complete spreading of all toes that was sustained for at least 2 s. The mice were examined twice with a time interval of 30 min between each session.

2.6.3. Grip strength test

Hindpaw grip strength was measured quantitatively using a grip strength meter (Biobeh), as described (Au et al., 2016; Meyer et al., 1979). In brief, the forepaws were rested on a wooden bar, and the hindpaws were positioned to grip a T-bar and pulled off. The value at which the mice released the bar in grams, as measured by the grip strength meter (Biobeh), was designated as the grip strength. Average grip strength values were obtained from a total of 5 measurements taken from two sessions with a 30-min time interval.

2.6.4. Electronic von Frey filament test

An electronic von Frey anesthesiometer (IITC, Woodland Hills, CA) was used to evaluate mechanical allodynia. Adult mice were habituated over three separate sessions with handling reduced to a minimum and placed on an elevated wire mesh platform in boxes made of the same mesh material for 30 min sessions. A rigid tip mounted on a force transducer probe was gently applied to the center of the hindpaw. The pressure was gradually increased for approximately 5 s, and the paw withdrawal threshold (PWT; in grams) was automatically recorded on the readout unit when the hindpaw was withdrawn (Cunha et al., 2004; Huehnchen et al., 2013; Martinov et al., 2013). The average of two values prior to injection was recorded as the baseline. For each animal, the final PWT at each time point was averaged from a total of 8 readings

(4 readings from each paw).

2.6.5. Cold allodynia

The acetone drop test was used to assess responses to innocuous cold stimuli, as described (Chine et al., 2019; Decosterd and Woolf, 2000). The mice were placed on elevated wire mesh platforms in boxes and allowed to habituate for 30 min, as for the pinprick assay and von Frey filament test. A drop of acetone solution was delicately dropped onto the lateral plantar surface of the hindpaw using a 1-ml syringe. The latency to respond including paw withdrawal, licking, biting or flinching within 1 min was recorded. Baseline values were taken on two alternate days prior to vincristine administration. On the experimental day, each mouse received six trials in total, and average values were calculated for each mouse.

2.7. Electrophysiological recording

Baseline recordings were taken before the first vincristine administration, and electrophysiological recordings were performed on a weekly basis after vincristine administration. The mice were anesthetized with ketamine (100 mg/kg) and xylazine (10 mg/kg) and placed on a heat pad to maintain a body temperature of 37 °C to avoid hypothermia during the course of recordings.

2.7.1. Sensory nerve action potential (SNAP) and nerve conduction velocity (NCV)

SNAP amplitudes and the NCV of the caudal nerve were recorded with a CerePlex Direct data acquisition system (Blackrock Microsystem), as described (Chine et al., 2019). Briefly, measurements were performed with filter settings of 250 Hz (high-pass) and 10 Hz (low-pass). The distance between the stimulation and recording electrodes was 5 cm, and a grounding electrode was placed between the stimulation and recording electrodes. Stimuli (0.2 ms) with a supramaximal stimulation intensity and a frequency of 1 Hz were used for measuring SNAPs and NCVs (AMPI Master 9). The SNAP parameter studied was the peak-to-peak amplitude (μ V), and the nerve conduction velocity (m/s) was derived from the onset latency (ms). All analyses were performed using Spike 2 software (Cambridge Electronic Design).

2.7.2. Electromyography recording

To record the compound muscle action potential (CMAP) from the proximal gastrocnemius muscle, the recording electrode was inserted subcutaneously into the gastrocnemius muscle, and the reference electrode was inserted into the Achilles tendon. Sciatic nerve was then stimulated (3 mA) at the sciatic notch with a frequency of 60 Hz with a grounding electrode placed at the base of the tail (Au et al., 2016). The CMAP was determined from the peak of negative deflection to the peak of positive deflection using Spike 2 software (Cambridge Electronic Design). For each animal, the mean CMAP amplitude was calculated from at least 6–8 peaks at each time point. The data are presented as the mean \pm SEM for each group.

2.8. Immunohistochemistry

At the endpoint of the behavioral tests, the mice were anesthetized and transcardially perfused with 4% PFA. The glabrous hindpaw skin (i.e., the electronic von Frey filament test site) and sciatic nerves were harvested, cryoprotected, and frozen in OCT compound (Tissue-Tek).

2.8.1. Intraepidermal nerve fiber (IENF) density quantification

IENF density in the hindpaw skin was quantified as described (Chine et al., 2019). Briefly, thirty-micron-thick sections perpendicular to the epidermis were cut serially with a cryostat. For each animal, five random fields from every fifth 30- μ m-thick section were selected for immunostaining with anti-protein gene product 9.5 (PGP9.5) primary antibodies (Ultraclone) to identify IENFs ($n = 5$ per group). IENFs that

crossed the dermal layer to reach the epidermis were counted, and the length (in mm) of the epidermal layer in each field was measured using ImageJ software to calculate the IENF density (i.e., number of IENFs/mm) (Boyette-Davis et al., 2011; Chine et al., 2019; Korngut et al., 2012).

2.8.2. Quantification of the total number of axons

The sciatic nerve was dissected from 5 mm proximal to the crush site to the level of the flexor retinaculum in the ankle. The nerves were then divided into 5-mm segments and cut into 4- μ m-thick transverse sections. The cryosections were immunostained with anti-neurofilament 200 (anti-NF-200; Millipore) primary antibodies. Images were taken at 20 \times magnification. The number of axons in the proximal 5-mm and distal 5-, 15-, and 25-mm segments was quantified using ImageJ software, as previously described (Au et al., 2016; Ma et al., 2011b). At least 7–9 images were quantified for each animal.

2.8.3. Myelin basic protein (MBP) immunoreactivity quantification

PFA-fixed sciatic nerves were segmented into 5, 15 and 25 mm distal to the sciatic notch and cut into 4- μ m-thick transverse sections. The cryosections were immunostained with anti-myelin basic protein (MBP) primary antibodies (Abcam). Images were captured using a Nikon Eclipse Ni-E epifluorescence microscope. The immunoreactivity of MBP was measured using ImageJ software and normalized to the total area of the nerve segment. The data are expressed as the percentage of MBP immunoreactivity per total area of the nerve segment (Chine et al., 2019; Painter et al., 2014).

2.9. Transmission electron microscopy (TEM)

For TEM, the sciatic nerves were dehydrated in a series of graded ethanol solutions, embedded in Spurr's resin, and sectioned (Chine et al., 2019). The ultrathin sections (70–80 nm) were stained with lead citrate and 2% uranyl acetate and mounted onto a carbon-coated 230-mesh copper grid. Micrographs were taken with a Philips Tecnai 12 BioTWIN, TSS microscope. Mitochondrial diameter in myelinated and unmyelinated axons was determined along the short axis using ImageJ software. The average mitochondrial diameter was obtained from at least 4–5 electron microscopy images per animal.

2.10. Measurement of mitochondrial membrane potential ($\Delta\psi_m$) in live DRG neurons

Two thousand DRG neurons were plated onto a poly-D-lysine/laminin-coated 35-mm glass-bottom dish (Ho et al., 2014) and allowed to grow for 17 h. Vincristine was first dissolved in PBS and then added to the cultures at a final concentration of 2.5 ng/ml, followed by a 3-h incubation at 37 °C. The total pool of mitochondria was labeled with 100 nM MitoTracker Green FM (Molecular Probes), and mitochondrial membrane potential was assessed using a mitochondria membrane potential-dependent dye, tetramethylrhodamine ethyl ester (TMRE) (Molecular Probes). After 30 min, the DRG cultures were washed with PBS and incubated with full NB medium for live-cell imaging. For each experimental condition, 10–15 images were randomly captured with a 63 \times objective using an inverted epifluorescence microscope (Nikon Ti-E) equipped with a motorized stage and incubator. MitoTracker Green FM staining was used to define the region of interest (ROI) for each mitochondrion, and the mitochondrial membrane potentials of the individual mitochondria were determined by the relative fluorescence intensity of TMRE measured in the 50 μ m of the neurites most distal from their adjacent cell bodies using ImageJ software with the Particle Analysis plugin (Zhou et al., 2016). Mitochondria with a TMRE fluorescence intensity > 50 A.U. were considered as TMRE-positive mitochondria. At least 400 mitochondria from > 70 distal axons were quantified in three separate experiments.

2.11. Detection of apoptosis using the TUNEL assay

To determine apoptotic cell death in DRG neurons in mice after treatment with vincristine, the terminal deoxynucleotidyl transferase dUTP nick-end labeling (TUNEL) assay was performed (*in situ* apoptosis detection kit; Chemicon) as described (Asthana et al., 2018; Chine et al., 2019). Briefly, lumbar 4, 5 and 6 (L4/5/6) DRGs, which directly supply the sciatic nerve, were dissected from hHsp27 Tg mice and their LMs 30 days after the first vincristine administration. Immunohistochemistry for TUNEL and PGP9.5 (Ultraclone) was performed on the same section to identify apoptotic neurons. Cryoprotected DRGs were cut into 5- μ m-thick cryosections, and every fourth DRG section was selected for the TUNEL assay. The DRG cryosections were treated with ice-cold ethanol/acetic acid (2:1 v/v) and immunostained with anti-PGP9.5 (Ultraclone) primary antibodies for the identification of neurons. The sections were then incubated with a reaction buffer containing terminal deoxynucleotidyl transferase at 37 °C for 60 min, treated with stop/wash buffer, and incubated with fluorescein-conjugated anti-digoxigenin at room temperature for 30 min. DAPI was used as a counterstain. Fluorescence images were taken with a 40 \times objective using a Nikon Eclipse Ni-E epifluorescence microscope. TUNEL- and PGP9.5-positive neurons with DAPI-labeled nuclei were counted. At least 10 sections per animal were analyzed.

2.12. Western blot analysis

L4/5/6 DRGs were dissected from both LM and hHsp27 Tg mice 30 days after the first vincristine administration for Western blot analysis, as previously described (Asthana et al., 2018; Chine et al., 2019). The DRGs were lysed and dissociated, and the protein concentration was determined using a BCA assay (Pierce). Protein lysates (20 μ g) were resolved on a 4–12% NuPAGE Bis-Tris gradient gel (Invitrogen) and transferred to a PVDF membrane. The PVDF membrane was incubated with 5% nonfat milk blocking buffer for 1 h, followed by incubation with anti-caspase-3 (1:1000; Cell Signaling Technology) primary antibodies, which detected both cleaved and total caspase-3 protein overnight at 4 °C, followed by incubation with secondary horseradish peroxidase-conjugated antibodies. Anti-GAPDH (1:1000; Santa Cruz Biotechnology Inc.) primary antibodies were used as loading controls. The immunoreactivity of each band was visualized using a West Femto Maximum Sensitivity Substrate Kit (Thermo Scientific). The band intensities were quantified using ImageJ software. Cleaved caspase-3 protein expression levels were first normalized to total caspase-3 levels and then normalized to GAPDH.

2.13. Calcium imaging

After 17 h of incubation, the culture medium of axotomized DRG neurons was replaced with artificial cerebrospinal fluid (aCSF) (composition in mM: 128.35 NaCl, 4 KCl, 0.58 NaH₂PO₄, 21 NaHCO₃, 30 d-glucose, 1.5 CaCl₂, and 1 MgSO₄) (Fletcher et al., 2017). A ratiometric calcium indicator dye, Fura-2-acetoxymethyl ester (Fura-2-AM), was applied to the cultured neurons at a final concentration of 2.5 μ M, and the neurons were incubated at 37 °C for 45 min. The cultures were then washed with prewarmed aCSF and incubated at 37 °C for 10 min before imaging. Bright-field images were first taken at 10 \times magnification using an inverted Nikon Eclipse Ti-S calcium imaging system. DRGs with phase-bright cell bodies and intact neurites were identified as healthy neurons, and the cell periphery of each DRG neuron was manually outlined and selected as ROI. In general, approximately 70–100 neurons were selected as ROIs from a single field. The neurons were excited with excitation wavelengths of 340 and 380 nm, respectively, and time-lapse images were taken every 2 s for 6 min with an emission filter of 510 nm using NIS-Elements software (Nikon). After 30 s, vincristine was added to the neurons at a final concentration of 10 ng/ml. After 5 min, KCl was added to the cultures at a final

concentration of 75 mM. The intracellular calcium concentration was expressed as the ratio of the fluorescence intensity upon excitation at 340 and 380 nm (i.e., F_{340/380}). The change in intracellular calcium transient ($\Delta F/F_0$) at each time point was calculated as the F_{340/380} ratio at that time point (i.e., ΔF) normalized to the basal F_{340/380} ratio of the same neuron at t = 0 (i.e., F₀). Only the KCl-responding cells (identified by a distinct sharp peak of $\Delta F/F_0$ immediately after KCl application) were included in the final dataset (Hill et al., 2018; Li et al., 2017). In all graphs, the data are presented as the mean \pm SEM from 3 independent experiments, and at least 100 neurons were quantified from each condition.

2.14. Statistical analysis

Animal behavior and electrophysiological data were analyzed by two-way ANOVA with repeated measures followed by post hoc Bonferroni's test. All other data were analyzed by either Student's *t*-test (for 2 experimental groups) or one-way ANOVA (for > 2 experimental groups) followed by post hoc Bonferroni's test where appropriate. The data are presented as the mean \pm SEM. Statistical analyses were performed by GraphPad Prism 6.0 software.

3. Results

3.1. Human Hsp27 protects against vincristine-induced poor axon regeneration and promotes functional recovery after peripheral nerve injury in vincristine-treated mice

CIPN patients experience a range of motor symptoms, including distal muscle weakness, gait impairments, and reduced balance and fine motor control. Peripheral nerve damage persists in CIPN patients since the slow recovery of damaged peripheral nerves does not always occur (Freilich et al., 1996; Peltier and Russell, 2002). Studies have demonstrated that chemotherapy drugs inhibit axon regeneration and reduce Schwann cell-promoting responses to sciatic nerve crush injury (Pan et al., 2003; Vuorinen and Roytta, 1990). For instance, DRG explant cultures treated with vincristine at concentrations ranging from 0.4 to 50 ng/ml reduced the neurite outgrowth of DRG neurons significantly (Au et al., 2014; Konings et al., 1994). We therefore first tested the protective effect of Hsp27 on axon regeneration in axotomized DRG neurons after treatment with vincristine. hHsp27-positive neurons were distinguished from non-hHsp27 neurons within the same DRG cultures by immunostaining with an anti-hHsp27 antibody (Ma et al., 2011b). Compared with non-hHsp27 neurons and LM controls treated with 0.5–10 ng/ml vincristine, in which the total neurite outgrowth was reduced by 30.4–81.2%, hHsp27-positive DRG neurons were protected from vincristine-induced neurite outgrowth inhibition significantly (Fig. 1A, B). There was no detectable effect on neuronal survival after treatment with relatively lower doses of vincristine (0.5–10 ng/ml) (Fig. 1C). However, at a higher dose (100 ng/ml), vincristine induced massive cell death in the DRG neurons of LM mice (38.7 \pm 0.4% of survival), whereas a majority of the DRG neurons in hHsp27 Tg mice were protected (68.8 \pm 0.5% of survival).

Mice usually regain full functional recovery within 1 month after sciatic nerve crush due to successful axon regeneration (Ma et al., 2011a); however, the presence of chemotherapy agents prevent the attempts of the injured axons to regenerate (Pan et al., 2003; Vuorinen and Roytta, 1990). To examine whether hHsp27 protects against the vincristine-induced inhibition of axon regeneration and facilitates *in vivo* functional recovery, we performed a battery of assays to test sensory (pinprick) and motor (toe spreading and grip strength) functional recovery on vincristine-treated hHsp27 Tg and LM mice after sciatic nerve crush (Fig. 2A). Adult mice were injected intraperitoneally with 0.05 mg/kg vincristine in two 5-day cycles with a 2-day break between cycles and were divided into three groups: LM + saline (LM mice injected with 0.9% saline), LM + vincristine, and hHsp27

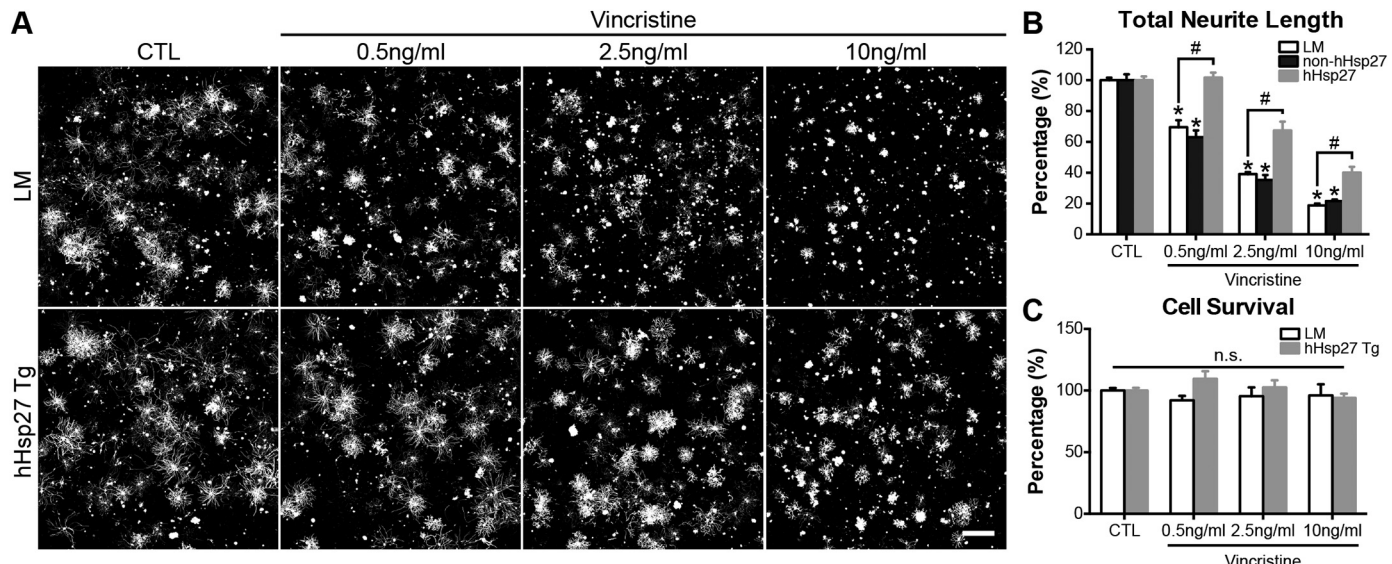


Fig. 1. Protective effect of hHsp27 on vincristine-induced neurite inhibition in cultured dorsal root ganglion (DRG) neurons.

Adult DRG neurons prepared from hHsp27 transgenic (Tg) mice and their age-matched wild type littermate (LM) were grown onto a poly-D-lysine/laminin-coated 8-well chamber slide for 17 h. (A) In LM DRG neurons, neurite outgrowth was markedly reduced in a dose-dependent manner after vincristine treatment. In contrast, DRG neurons from hHsp27 Tg mice exhibited significantly longer neurites than LM mice. Saline was used as vehicle control. Scale bar, 500 μm. (B) Average total neurite length was quantified using automated WIS-NeuroMath software (Weizmann Institute of Science, Israel), normalized with respective controls in each individual experiment and expressed as percentage. hHsp27-expressing neurons exhibited significantly longer neurites when compared with LM and non-hHsp27-expressing neurons. (C) Vincristine treatment did not affect cell survival of DRG neurons at all tested concentrations, and neurons remained healthy. Mean ± SEM of triplicates. * $P < .05$, ** $P < .05$; one-way ANOVA, followed by post hoc Bonferroni's test. CTL, control; n.s., not significant.

Tg + vincristine. We performed sciatic nerve crush on day 12 after the first injection, and the LM mice recovered much slower than the hHsp27 Tg mice after vincristine treatment, as measured by the pin-prick assay. The daily sensory recovery of the hHsp27 Tg mice was comparable to that of the vehicle (saline)-treated controls. The LM mice started to show the first sensory responses on day 11, while the hHsp27 Tg mice showed responses on day 9 (Fig. 2B). Strikingly, full motor function recovery, such as toe spreading (reaching score 2), was significantly delayed by 8–10 days in the LM mice when compared with the hHsp27 Tg and vehicle-treated control mice (Fig. 2C). The motor grip strength of the LM mice was consistently lower than that of hHsp27 Tg and saline-treated control mice from day 5 to 31 after sciatic nerve crush injury. The vincristine-treated LM mice returned to baseline values on day 35, which was 11 days later than the hHsp27 Tg and saline control mice (Fig. 2D). We next performed electromyography (EMG) recording, which allows the detection of functional neuromuscular synaptic transmission in distal target muscles, during the course of recovery to assess functional synapse formation following crush injury. The CMAP of the gastrocnemius muscle was evaluated on a weekly basis after crush injury. The CMAP amplitudes in the vincristine-treated hHsp27 Tg mice were maintained at a comparable level to those of the saline-treated mice. However, the vincristine-treated LM mice took 3 more weeks to return to baseline CMAP values, which was consistent with our animal behavior data (Fig. 2E).

3.2. Human Hsp27 reverses vincristine-induced neuropathic pain symptoms and preserves distal afferent nerve fibers in the footpad

Next, we assessed the *in vivo* protective effects of hHsp27 using an animal model of vincristine-induced peripheral neuropathy. To induce CIPN, adult male mice were i.p. injected with vincristine to develop CIPN symptoms, such as mechanical and cold hypersensitivity, as measured by the electronic von Frey and acetone drop tests, respectively (Fig. 3A). In the LM mice, vincristine reduced the threshold for mechanical stimuli to elicit a hindpaw withdrawal response (i.e., PWT) by nearly half compared to that resulting from vehicle treatment on day

7 after the first injection (2.68 ± 0.24 g vs 5.32 ± 0.33 g baseline value), and this effect was sustained for 4 weeks. Nevertheless, the development of mechanical allodynia was completely prevented in the hHsp27 Tg mice, as the PWT values in the vincristine-treated hHsp27 Tg mice were comparable with those in vehicle-treated controls throughout the entire course of the experiment (Fig. 3B). We also performed an acetone drop test to quantify cold allodynia, and we observed a significant increase in response time to the application of acetone to the hindpaws in the LM mice only. The LM mice developed a marked hypersensitivity to acetone and exhibited a significantly withdrawal duration of 6.02 ± 1.02 s on day 13 after vincristine treatment. Acetone continued to elicit a sustained flexion throughout the study. Strikingly, the response time to application of acetone in the vincristine-treated hHsp27 Tg mice was maintained at the baseline level throughout the study time course, and this was comparable to the vehicle-treated controls (Fig. 3C). This clearly indicates that forced expression of hHsp27 completely prevented the development of mechanical and cold hypersensitivity.

IENFs are free distal nerve endings arising predominantly from unmyelinated (C-fibers) and to a lesser extent from thinly myelinated (A delta fibers) sensory neurons within the dermis. IENFs are important for conveying pain and temperature information, and the loss of IENF was evident in rat models of CIPN treated with cisplatin, oxaliplatin, paclitaxel and vincristine (Boyette-Davis and Dougherty, 2011; Boyette-Davis et al., 2011; Lauria et al., 2005; Siau and Bennett, 2006). We therefore examined whether hHsp27 prevents distal axonal loss in the footpad, the location of the nerve endings of nociceptive neurons that innervate the epidermis and the primary allodynia testing site. In the LM mice, the IENF density was dramatically decreased by 43.3% on day 30 after the first injection of vincristine, a time point at which mechanical and cold allodynia persisted in our behavioral assessment. Strikingly, IENFs were well preserved in the hHsp27 Tg mice (73.25 ± 4.49), even after vincristine treatment, as the IENF density was comparable to that of the vehicle-treated controls (78.47 ± 5.5) (Fig. 4A, B). To further confirm the protective effect of hHsp27 on the degeneration of afferent nerve fibers, we quantified the number of NF-

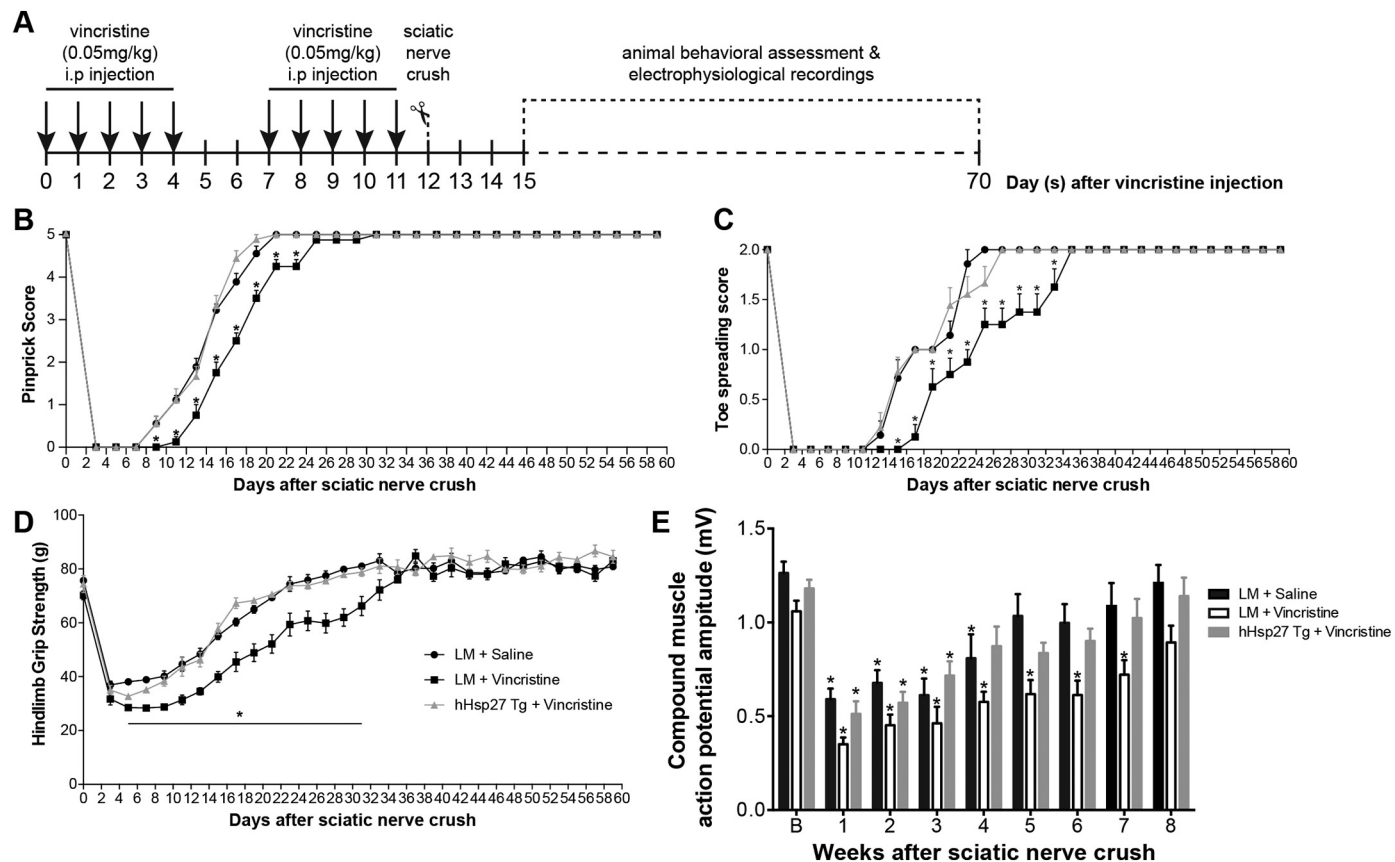


Fig. 2. hHsp27 protects against vincristine-induced delay in sensory and motor functional recovery following sciatic nerve crush. (A) Schematic diagram showing the timeline of vincristine treatment and sciatic nerve crush. hHsp27 Tg and their age-matched wild type LM mice were administered with a total 10 injections of vincristine (0.05 mg/kg) at days 0–4, and days 7–11. Sciatic nerve crush injury was performed on the left sciatic nerve at day 12. Sensory and motor functional recovery were monitored by a battery of animal behavioral tests for 2 months. (B) Sensory functional recovery, as assessed by pinprick sensory assay, was markedly delayed in vincristine-treated LM mice. Strikingly, the daily sensory recovery of hHsp27 Tg mice was comparable to vehicle controls (saline). (C) Full motor function recovery such as toe spreading (reaching score 2) was significantly delayed by 8–10 days in LM mice when compared with hHsp27 Tg and vehicle control mice. (D) The grip strength of hindlimbs was significantly reduced in vincristine-treated LM mice from days 5 to 31 when compared with vincristine-treated hHsp27 Tg mice and saline-treated mice. (E) Electromyography recording showed that vincristine-treated LM mice displayed a significant reduction in compound muscle action potential (CMAP) amplitudes, while the vincristine-treated hHsp27 Tg mice showed comparable CMAP amplitudes to saline-treated controls. Mean \pm SEM ($n = 9$ mice per group); * $P < .05$, two-way repeated measures ANOVA, followed by post hoc Bonferroni's test. B, baseline.

200-positive axons in the distal segments of the sciatic nerve after vincristine treatment. Thirty days after the first injection of vincristine, we observed a marked reduction in NF-200-positive axons in the nerve segments at 15 mm and 25 mm distal to the sciatic notch, but only in the vincristine-treated LM mice (Fig. 4C). The vincristine-treated hHsp27 Tg mice exhibited a comparable number of NF-200-positive axons to the vehicle-treated controls (Fig. 4D).

3.3. hHsp27 protects against vincristine-induced demyelination and restores sensory nerve action potential

It has been suggested that nerve conduction studies can be used to objectively assess the extent of peripheral nerve damage secondary to chemotherapy in animal models and patients (Boehmerle et al., 2014; Chaudhry et al., 1994). Axonal degeneration and demyelination result in slowing of the nerve conduction velocity and are key pathological features of vincristine-induced peripheral neuropathy that are directly associated with the development of neuropathic pain (Boehmerle et al., 2014; Geisler et al., 2016; Windebank and Grisold, 2008). We therefore performed a detailed histological analysis of myelination and nerve conduction velocity (NCV) studies to validate the protective effect of hHsp27 against the mechanical and cold allodynia observed in the behavioral tests. We first quantified MBP immunoreactivity in transverse sections of the sciatic nerve 5–25 mm distal to the sciatic notch

(Asthana et al., 2018), and we found a loss of MBP immunoreactivity (47–62% reduction), indicating massive demyelination, 30 days after vincristine treatment. Remarkably, forced expression of hHsp27 completely protected against vincristine-induced demyelination. In contrast to the uniform distribution of MBP immunoreactivity in the sciatic nerve transverse sections of the hHsp27 mice and vehicle-treated controls, the vincristine-treated LM mice showed a nonuniform distribution with axons that lacked MBP expression (Fig. 5A). The quantitative analysis of MBP immunoreactivity in segments of the sciatic nerve 5, 15 and 25 mm distal to the sciatic notch demonstrated a consistent and significant reduction of myelination along the sciatic nerve in the vincristine-treated LM mice but not in the hHsp27 Tg mice (Fig. 5B). Consistent with these findings, TEM analysis of the ultrastructure of the sciatic nerve revealed significant demyelination in the vincristine-treated LM mice, as indicated by rupture of the myelin sheath; the myelin sheath structure remained largely intact in the hHsp27 Tg mice after vincristine treatment (Fig. 5C).

The progression of CIPN is associated with a significant reduction in both SNAP and NCV, while the latter confirms axonal degeneration and demyelination. Vincristine induces degeneration of unmyelinated and myelinated sensory fibers as well as progressive sensory peripheral neuropathy, which is characterized by decreased SNAP amplitudes of the caudal nerve (Boehmerle et al., 2014; Geisler et al., 2016; Van Helleputte et al., 2018). In the current study, we observed a significant

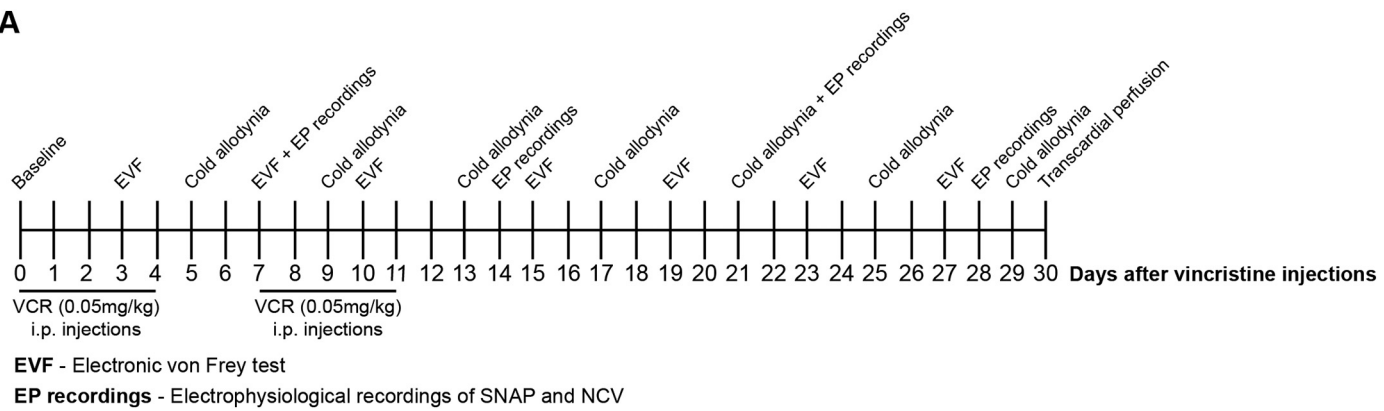
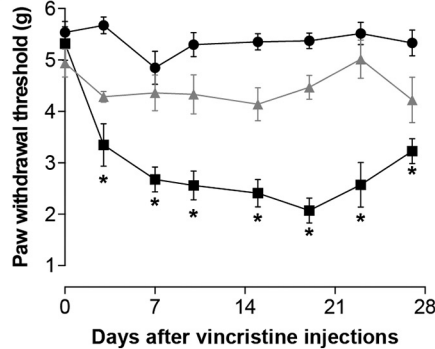
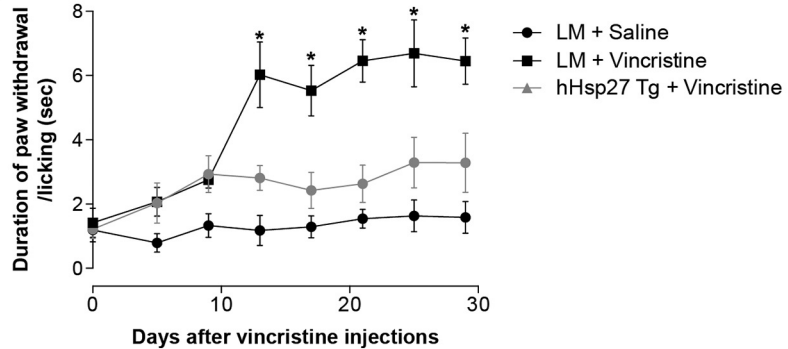
A**B****C**

Fig. 3. hHsp27 completely prevents the development of chemotherapy-induced peripheral neuropathy symptoms after vincristine treatment.

(A) Schematic diagram showing timeline for electronic von Frey (EVF), acetone drop test, and electrophysiological recordings of sensory nerve action potential (SNAP) and nerve conduction velocity (NCV). Adult mice were injected intraperitoneally with 0.05 mg/kg vincristine in two 5-day cycles with 2-day break between cycles and divided into three groups including LM + saline, LM + vincristine, and hHsp27 Tg + vincristine. Baseline behavior values and electrophysiology recordings were taken after habituations. Electrophysiological recordings were performed on a weekly basis until day 28 after the first vincristine injection. (B) EVF was used for assessing mechanical allodynia. LM mice developed severe and irreversible mechanical allodynia after the first vincristine injection. In contrast, hHsp27 Tg mice were protected from vincristine-induced mechanical allodynia during the entire course of the experiment. (C) Acetone drop test was used for assessing cold allodynia. LM mice developed significant cold allodynia at day 13 and sustained until day 29 after the first vincristine injection. However, hHsp27 Tg did not exhibit any sign of cold allodynia during the entire course of the experiment. Mean \pm SEM ($n = 7$ mice per group); * $P < .05$, two-way repeated measures ANOVA, followed by post hoc Bonferroni's test.

reduction in the SNAP amplitudes (Fig. 5D) and NCV (Fig. 5E) of the caudal nerve 7 days post vincristine treatment, which is in line with the onset of CIPN symptoms and axonal pathology, as shown in Figs. 3–5 and other studies (Boehmerle et al., 2014; Geisler et al., 2016; Van Helleputte et al., 2018). Forced expression of hHsp27 blocked the development of electrophysiological deficits caused by vincristine treatment. In the hHsp27 Tg mice, the SNAP amplitude and conduction velocity were not significantly different from those of the vehicle-treated controls after vincristine treatment (Fig. 5D, E). These findings are consistent with our histological data demonstrating preservation of axon number and myelination in the hHsp27 Tg mice.

3.4. hHsp27 preserves mitochondrial integrity by preventing mitochondrial swelling and loss of mitochondrial membrane potential in axon fibers

Accumulating evidence has suggested that mitochondrial dysfunction and toxicity (mitotoxicity) could be the primary cause of CIPN symptoms induced by chemotherapeutic agents, including vincristine, paclitaxel, oxaliplatin and bortezomib (Bennett et al., 2011; Canta et al., 2015; Flatters and Bennett, 2006; Xiao and Bennett, 2008). Mitotoxicity results in morphological abnormalities in the form of swollen and vacuolated mitochondria, resulting in a calcium imbalance, as mitochondria buffer calcium loads to maintain calcium homeostasis in cells (Canta et al., 2015; Flatters and Bennett, 2006; Siau and Bennett, 2006). Primary superior cervical ganglion neurons treated with

vinblastine, a chemical analogue of vincristine that also induces CIPN, decreases the mitochondrial membrane potential, leading to neuronal apoptosis, in cultures (Ikegami and Koike, 2003). To investigate the potential protective effects of hHsp27 on mitochondrial integrity, we first performed ultrastructural morphometric analyses of mitochondria in myelinated and unmyelinated axons 30 days after vincristine treatment using TEM and observed swollen mitochondria in the distal sciatic nerves of vincristine-treated LM mice when compared with the mitochondria in hHsp27 Tg mice and vehicle-treated controls (Fig. 6A, B). In the vincristine-treated LM mice, the diameter of the mitochondria in both myelinated and unmyelinated axons was dramatically increased by 32% and 36%, respectively, when compared with that in the vehicle-treated controls. In contrast, the diameter of the mitochondria in sciatic nerves from the hHsp27 Tg mice was comparable to that in the vehicle-treated controls, suggesting that hHsp27 protected myelinated and unmyelinated axons from mitochondrial swelling (Fig. 6C, D). We then measured the axonal mitochondrial membrane potential in DRG neurons with the fluorescent dye TMRE by live-cell imaging. Depolarized or damaged mitochondria have decreased mitochondrial membrane potential and fail to sequester TMRE, hence reduced the uptake of TMRE (Zhou et al., 2016). We observed a rapid loss of TMRE fluorescence (decreased by 65%) in the distal axons of DRG neurons from the LM mice after treating with vincristine. Strikingly, the loss of TMRE fluorescence was largely prevented in vincristine-treated DRG neurons from the hHsp27 Tg mice and was restored to a level comparable to that

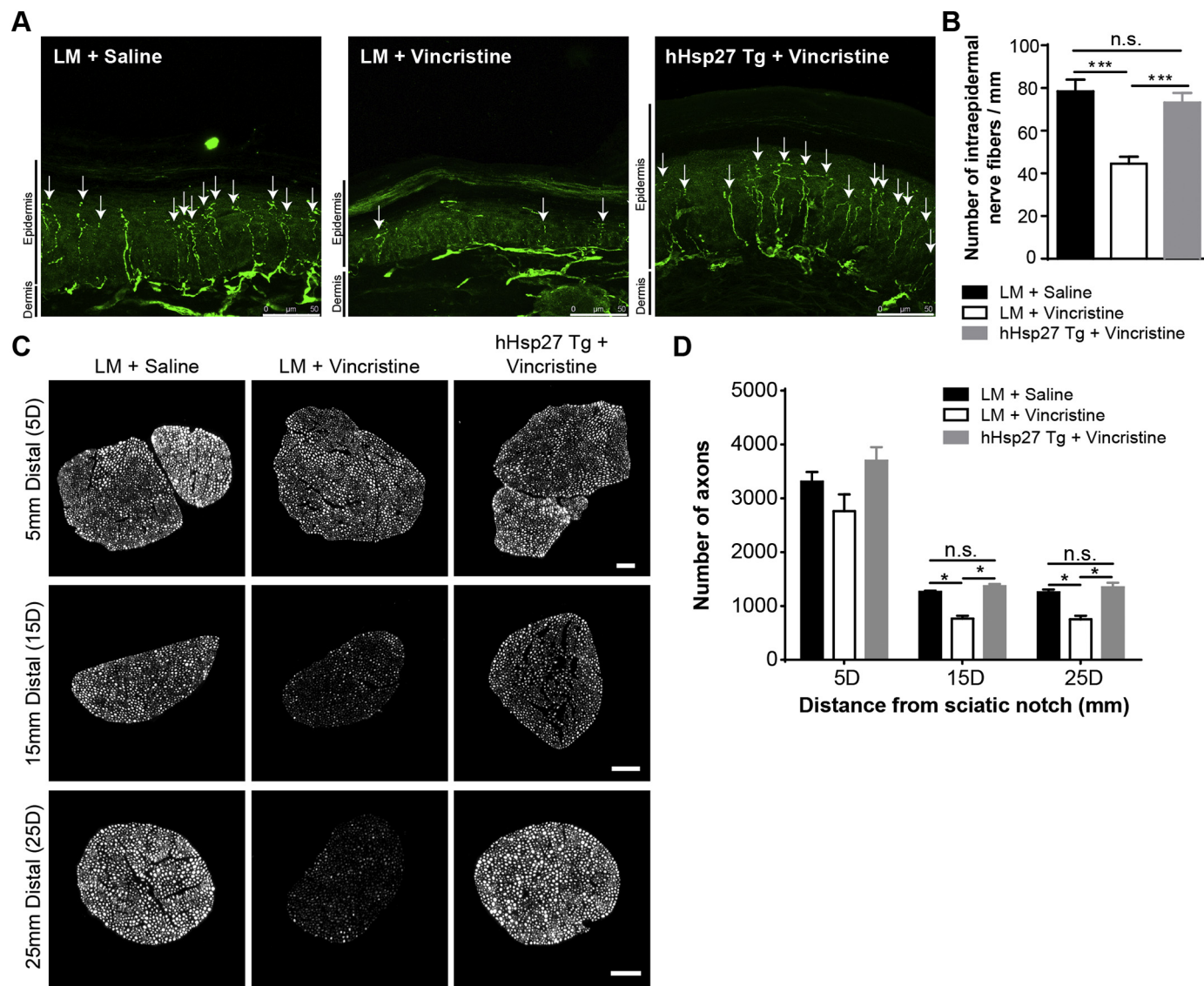


Fig. 4. hHsp27 protects sensory nerve fibers against vincristine-induced loss.

(A) Representative confocal images showed that intraepidermal nerve fibers (IENFs) immunostained for anti-PGP9.5 antibodies in lateral hindpaws where the mechanical allodynia testing site was located. Scale bar, 50 μm. (B) IENF density was dramatically reduced in LM mice, while IENFs were well preserved in hHsp27 Tg mice at a level comparable to saline-treated control mice. Mean ± SEM ($n = 6\text{--}9$ mice per group); *** $P < .001$, two-way ANOVA, followed by post hoc Bonferroni's test. (C, D) The number of NF-200-positive axonal fibers at 15 mm- and 25 mm-distal to sciatic notch was significantly lost in LM mice only. Vincristine-treated hHsp27 Tg mice showed comparable number of NF-200-positive axons to vehicle controls. Mean ± SEM ($n = 3$ mice per group); * $P < .05$, two-way ANOVA, followed by post hoc Bonferroni's test. n.s., not significant.

of the saline-treated LM controls (Fig. 6E, F). The percentage of TMRE/MitoTracker Green-positive mitochondria was also reduced by 77% in the axonal mitochondria of vincristine-treated LM mice, whereas the number of TMRE/MitoTracker Green-positive mitochondria were returned to nearly control levels in the hHsp27 Tg mice after vincristine treatment (Fig. 6G).

3.5. hHsp27 protects DRG neurons from apoptosis by inhibiting vincristine-induced caspase-3 activation

Vincristine-induced mitochondrial dysfunction induces the release of cytochrome *c* and the activation of the caspase-3 apoptotic cascade in cultured neurons (Ikegami and Koike, 2003). Pharmaceutical agents intended to reduce vincristine-induced neuronal apoptosis protect neurons from axonal degeneration *in vitro* (Wang et al., 2000) and prevent CIPN symptoms induced by paclitaxel *in vivo* (Wang et al., 2004). It has been shown that Hsp27 exerts strong anti-apoptotic effects

on DRG neurons by preventing cytochrome *c* release (Concannon et al., 2003; Costigan et al., 1998). These studies prompted us to examine whether hHsp27 protects sensory neurons from apoptosis after vincristine treatment in mice. We first examined the number of apoptotic DRG neurons using the TUNEL assay 30 days after vincristine treatment (Fig. 7A) (Asthana et al., 2018). In line with a previous study (Ikegami and Koike, 2003), we detected a higher number of TUNEL- and PGP9.5-positive neurons in the vincristine-treated LM mice than in the hHsp27 Tg mice (Fig. 7B). We hypothesized that the reduced level of neuronal apoptosis in the hHsp27 Tg mice was associated with the inactivation of caspase-3 after vincristine treatment. We therefore examined the protein expression of cleaved caspase-3 (i.e., the most critical downstream effector of the apoptotic cascade) in L4/5/6 DRGs, which directly supply the sciatic nerve, 30 days after vincristine treatment. Vincristine induced a 4.5-fold increase in cleaved caspase-3 protein expression in the LM mice, but there was no detectable cleaved caspase-3 expression in the hHsp27 Tg and saline-treated mice

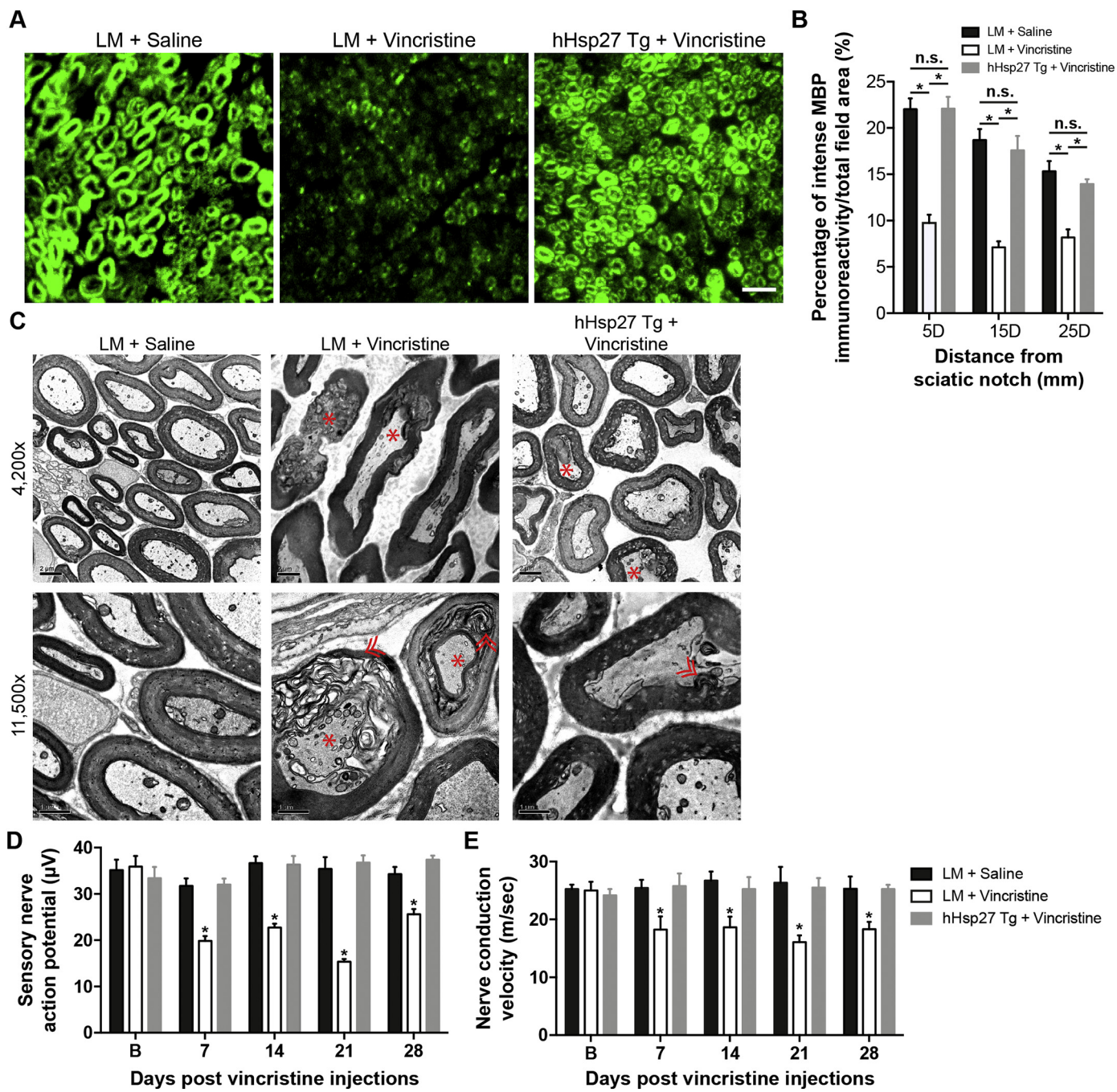
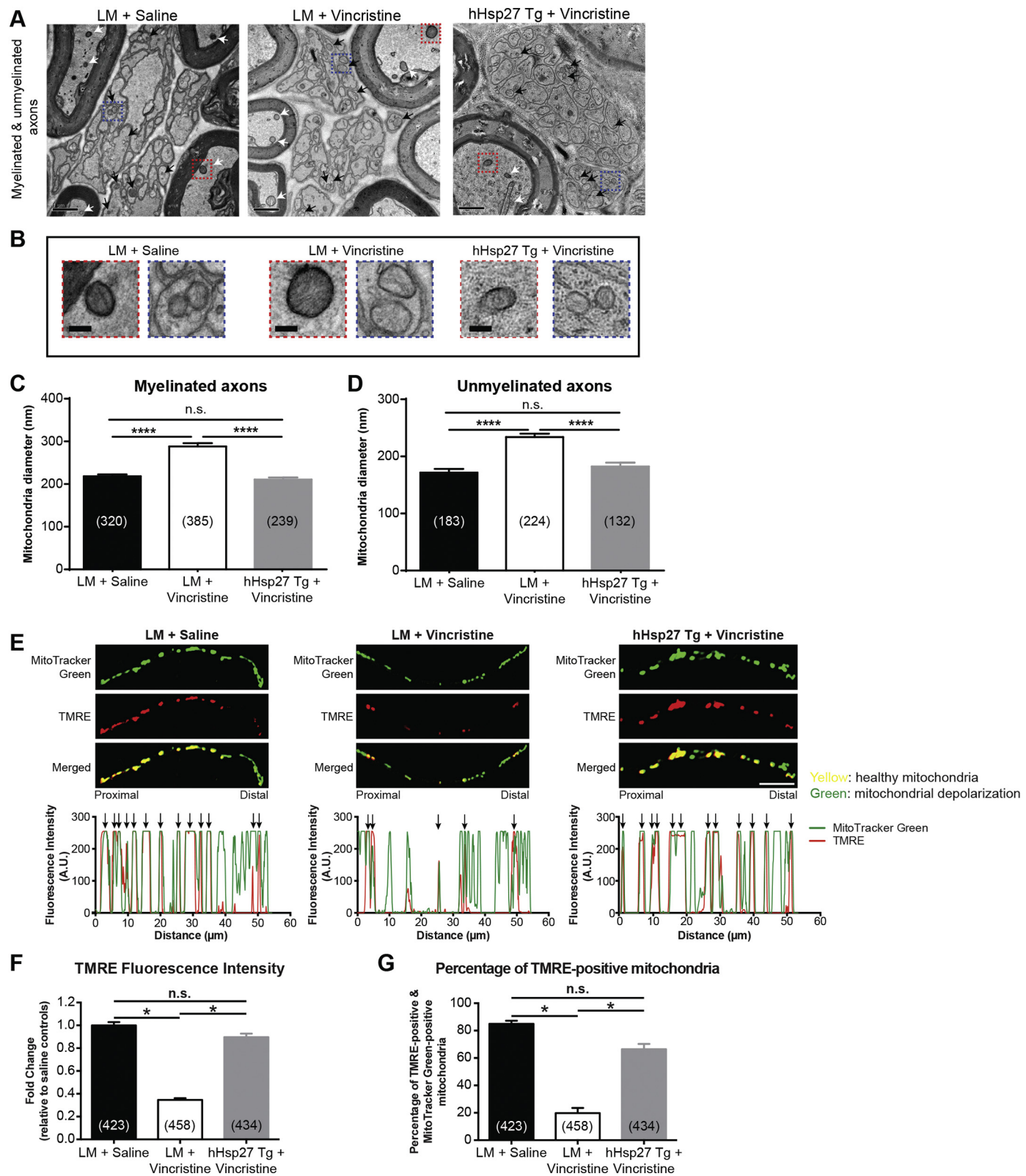


Fig. 5. hHsp27 prevents vincristine-induced demyelination in sciatic nerve, and restores sensory nerve action potential (SNAP) and nerve conduction velocity (NCV). (A) Four-micron thick transverse sections of sciatic nerves were immunostained for anti-myelin basic protein (MBP) antibodies 30 days after vincristine treatment. Scale bar, 10 μm. (B) Immunoreactivity of MBP was quantified and presented as percentage of intense MBP immunofluorescence per total field area. Vincristine induced a marked reduction in MBP immunoreactivity indicating massive demyelination occurred 30 days after vincristine treatment in LM mice only. Remarkably, forced expression of hHsp27 completely protected against the vincristine-induced demyelination by showing uniform distribution of MBP immunoreactivity similar to saline controls. Mean ± SEM ($n = 4$ mice per group, 3–5 field in every 3rd section); $*P < .05$, one-way ANOVA, followed by post hoc Bonferroni's test. (C) Representative transmission electron microscopy (TEM) images revealed intensive axonal degeneration (red asterisks) and demyelination (red double arrowheads) in LM mice. Scale bars, 2 μm (upper panel), 1 μm (lower panel). (D) In LM mice, SNAP amplitudes of the caudal nerve were markedly reduced at 1 week after the first vincristine injection and sustained throughout the entire study period. In contrast, SNAP amplitudes in vincristine-treated hHsp27 Tg mice were maintained at baseline levels throughout the entire study period. (E) NCV was markedly reduced in LM mice 1 week after the first vincristine injection, while hHsp27 Tg maintained their NCV at baseline level throughout the entire study period. Mean ± SEM ($n = 4$ –6 mice per group); $*P < .05$, two-way repeated measures ANOVA, followed by post hoc Bonferroni's test. D, distal; n.s., not significant.



(caption on next page)

(Fig. 7C). These results collectively support the anti-apoptotic role of hHsp27 in a mouse model of CIPN in preventing vincristine-induced neuronal apoptosis via modulating the caspase-3 apoptotic cascade.

3.6. hHsp27 attenuates intracellular calcium influx in primary DRG neurons after vincristine treatment

Growing evidence suggests that disruption of intracellular calcium homeostasis in neurons due to off-target effects of chemotherapy drugs leads to the pathogenesis and development of sensory disturbances in

Fig. 6. hHsp27 preserves mitochondrial integrity by preventing mitochondrial swelling and loss of mitochondrial membrane potential in axon fibers. (A, B) Ultrastructural morphometry analysis using transmission electron microscopy (TEM) demonstrated swelling of mitochondria in vincristine-treated LM mice. Scale bar: 1 μm in A and 250 nm in B. (C, D) The mitochondria diameter of (C) myelinated and (D) unmyelinated was significantly increased in LM mice, indicating significant mitochondrial swelling. The diameter of mitochondria in sciatic nerve of hHsp27 Tg mice remained comparable to saline controls. Mitochondria diameter was averaged from at least 120 mitochondria. Mean ± SEM ($n = 3\text{--}4$ mice per group). (E) Vincristine induced a rapid loss of mitochondrial membrane potential indicated by reduction of TMRE fluorescence in distal axons of cultured LM DRG neurons. In contrast, forced expression of hHsp27 preserved mitochondrial membrane potential after vincristine treatment. Arrows indicated TMRE-positive and MitoTracker Green-positive (i.e. healthy) mitochondria. Scale bar: 10 μm. (F) Quantification of TMRE fluorescence intensity in MitoTracker Green-positive mitochondria using ImageJ software with Particle Analysis plugin. Vincristine induced a massive loss of TMRE fluorescence intensity in axonal mitochondria of LM DRG neurons. In contrast, the loss of TMRE fluorescence was largely prevented in vincristine-treated DRG neurons from the hHsp27 Tg mice. (G) In vincristine-treated LM DRG neurons, the number of TMRE-positive and MitoTracker Green-positive mitochondria was markedly reduced, which indicated mitochondrial depolarization. The number of TMRE-positive and MitoTracker Green-positive mitochondria in hHsp27 Tg DRG neurons was comparable to saline-treated LM controls. More than 400 mitochondria were quantified in three separated experiments. Mean ± SEM in triplicate. * $P < .05$, *** $P < .0001$, one-way ANOVA, followed by post hoc Bonferroni's test. n.s., not significant.

CIPN patients. Reducing intracellular calcium influx has been shown to effectively ameliorate CIPN symptoms induced by chemotherapeutic agents (Flatters and Bennett, 2004; Muthuraman et al., 2008; Siau and Bennett, 2006; Xiao et al., 2007). However, the precise role of the intracellular calcium concentration in CIPN is not yet understood. We therefore monitored the intracellular calcium level in primary DRG neurons by live-cell fluorescence imaging. Fura-2-AM is a widely used ratiometric fluorescent dye for calcium imaging, and the ratio of the fluorescence intensities obtained by excitation at 340 and at 380 nm ($\Delta F/F_0$) was used to calculate the intracellular calcium level (Boehmerle et al., 2006). DRG neurons treated with vincristine showed an initial peak and a subsequent sustained phase of calcium influx (Fig. 8A, B). To quantify the calcium influx of each single neuron following vincristine treatment, we calculated the area under the curve (AUC) of the Fura-2 traces. The AUC is expressed in arbitrary units and represents the total amount of calcium influx after vincristine treatment. The magnitude of calcium influx was significantly reduced in the hHsp27 DRG neurons when compared with the LM neurons (Fig. 8C). We also quantified the number of neurons that responded with a distinct peak following vincristine treatment, and the number of vincristine-responding neurons in the DRG cultures from the LM mice was 34.1% higher than that in the DRG cultures from the hHsp27 mice (Fig. 8D).

4. Discussion

Vincristine is one of the most widely used chemotherapeutic agents for treating a range of solid carcinomas, despite the fact that CIPN is the most severe and undesirable off-target effect of chemotherapy. CIPN can result in chemotherapy dose reduction to a suboptimal level or even discontinuation of chemotherapy. The early symptoms of vincristine-induced CIPN are mainly sensory disturbances, including numbness, tingling, paraesthesia and painful sensation in the upper and lower limbs. Motor dysfunctions, including loss of tendon reflexes, muscle cramping and weakness in distal muscles, often occur at advanced stages (Quasthoff and Hartung, 2002; Staff et al., 2017). In some cases, the symptoms are irreversible, even though some of them can be partially resolved within months after treatment withdrawal. For decades, multiple drugs have been used and studied to prevent and treat CIPN; however, the results of these efforts have been largely disappointing. Variations in CIPN assessment and diagnosis limiting comparability, the variety of treatment paradigms used in clinical trials and complex drug-drug interactions have made interpretations a major challenge. Duloxetine, which has been demonstrated clinically to improve pain, is the only agent recommended by The American Society of Clinical Oncology for the treatment of established paclitaxel- and oxaliplatin-induced CIPN with (Hershman et al., 2014). Potential preventive agents such as ethosuximide (a calcium channel blocker) and lacosamide (an analgesic drug) only partially improve vincristine-induced mechanical and cold allodynia but are unable to prevent vincristine-induced axonal degeneration. Ethosuximide rapidly relieves mechanical and cold allodynia in vincristine-treated rats; however, CIPN symptoms relapse 24 h after

administration (Flatters and Bennett, 2004). Lacosamide prevents the development of cold allodynia but fails to protect the rats from mechanical allodynia after vincristine treatment (Geis et al., 2011). Nevertheless, there is currently no agent that has demonstrated significant clinical efficacy in preventing CIPN.

Our recent study demonstrated the protective role of Hsp27 on paclitaxel-induced axonal degeneration, neuronal apoptosis, mitochondrial swelling in distal nerves, and demyelination, resulting in the prevention of mechanical and cold allodynia in a mouse model of paclitaxel-induced peripheral neuropathy (Chine et al., 2019). We hypothesized that Hsp27 is also effective in preventing vincristine-induced CIPN. In the current study, we further demonstrated that forced expression of hHsp27 in peripheral neurons can overcome the adverse effects of vincristine in two mouse models of peripheral nerve injury, namely, sciatic nerve crush and CIPN. Chemotherapeutic drugs that cause CIPN, such as paclitaxel, can elicit axonal degeneration similar to that observed after mechanical axon injury, such as sciatic nerve crush injury, which was used in the current study (Fukuda et al., 2017; Gornstein and Schwarz, 2014; Wang et al., 2002; Wang et al., 2004). Our data showed that hHsp27 protects neurons against axonal degeneration, demyelination, mitochondrial dysfunction, and apoptosis after vincristine treatment. More importantly, we demonstrated for the first time that vincristine-induced calcium influx is markedly attenuated by neuronal expression of hHsp27.

Calcium, a major signaling molecule in eukaryotic cells, is involved in a wide range of physiological processes, such as release of neurotransmitters, phosphorylation and dephosphorylation of membrane proteins (i.e., enzymes), and transcriptional regulation. Calcium is also a key regulator of axonal degeneration in many pathological conditions. Under normal circumstances, neurons maintain consistent levels of intracellular calcium in the nanomolar range through multiple signaling pathways that modulate the release of intracellular calcium and the influx of extracellular calcium. In addition to generating energy in the form of ATP, mitochondria play an indispensable role in maintaining intracellular calcium levels under physiological conditions (Berridge, 1998; Gleichmann and Mattson, 2011). In cultured DRG neurons, intracellular calcium levels rapidly increase at the injury site and neuronal soma immediately after laser axotomy (Avery et al., 2012; Cho et al., 2013). It has been reported that rapid calcium influx triggers the fragmentation and degeneration of injured axons, a process known as Wallerian degeneration (Vargas et al., 2015). It is evident that Wallerian degeneration and subsequent axonal loss induced by peripheral nerve injuries can be prevented by overexpression of a *Wld^s* (i.e., slow Wallerian degeneration) mutant in mice (Coleman and Freeman, 2010). Further studies have demonstrated that delayed axonal degeneration in *Wld^s*-expressing neurons is due largely to the suppression of injury-induced calcium influx (Avery et al., 2012; Vargas et al., 2015). Overexpression of the calcium-binding protein parvalbumin protects axons from fragmentation by blocking calcium influx into injured neurons, resulting in delay of Wallerian degeneration (Vargas et al., 2015). Compelling evidence has suggested that dysregulation of calcium homeostasis results in the development of various neuropathic pain

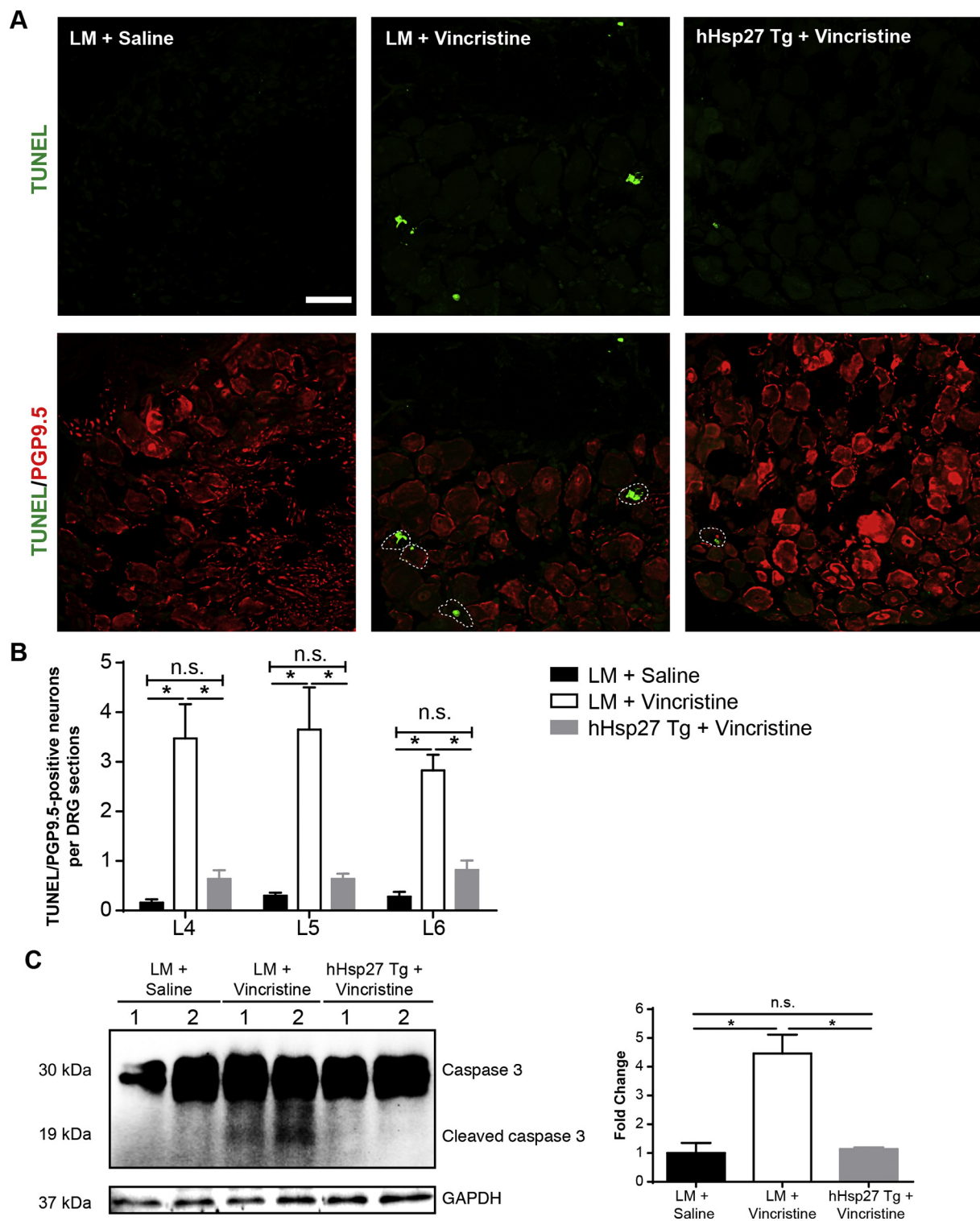


Fig. 7. hHsp27 protects DRG neurons from apoptosis by inhibiting vincristine-induced caspase 3 activation.

(A) TUNEL assay was performed on 5-μm-thick cryosections of lumbar 4 (L4), L5 and L6 DRG neurons, which directly supply the sciatic nerve, 30 days after vincristine treatment. Scale bar, 50 μm. (B) A significantly higher number of TUNEL and PGP9.5-positive neurons were detected in vincristine-treated LM DRG sections than in the hHsp27 Tg DRGs. (C) Western blot analysis revealed that vincristine induced a 4.5-fold increase in cleaved caspase 3 protein expression in L4/5/6 DRGs of LM mice, while there was no detectable cleaved caspase 3 expression in hHsp27 Tg and saline-treated mice. Mean ± SEM ($n = 3\text{--}4$ mice per group); * $P < .05$, one-way ANOVA, followed by post hoc Bonferroni's test. n.s., not significant.

conditions, including CIPN (Jaggi and Singh, 2012; Starobova and Vetter, 2017). Intraperitoneal administration of vincristine in rats increases the total calcium level in the sciatic nerve dramatically (Kaur et al., 2010; Muthuraman et al., 2008). Paclitaxel, a commonly used

antineoplastic agent for treating solid carcinomas, promotes excessive tubulin polymerization as well as rapidly increases intracellular calcium levels in human SH-SY5Y cells (Boehmerle et al., 2006). Prolonged exposure to paclitaxel and vincristine alters the function of the calcium

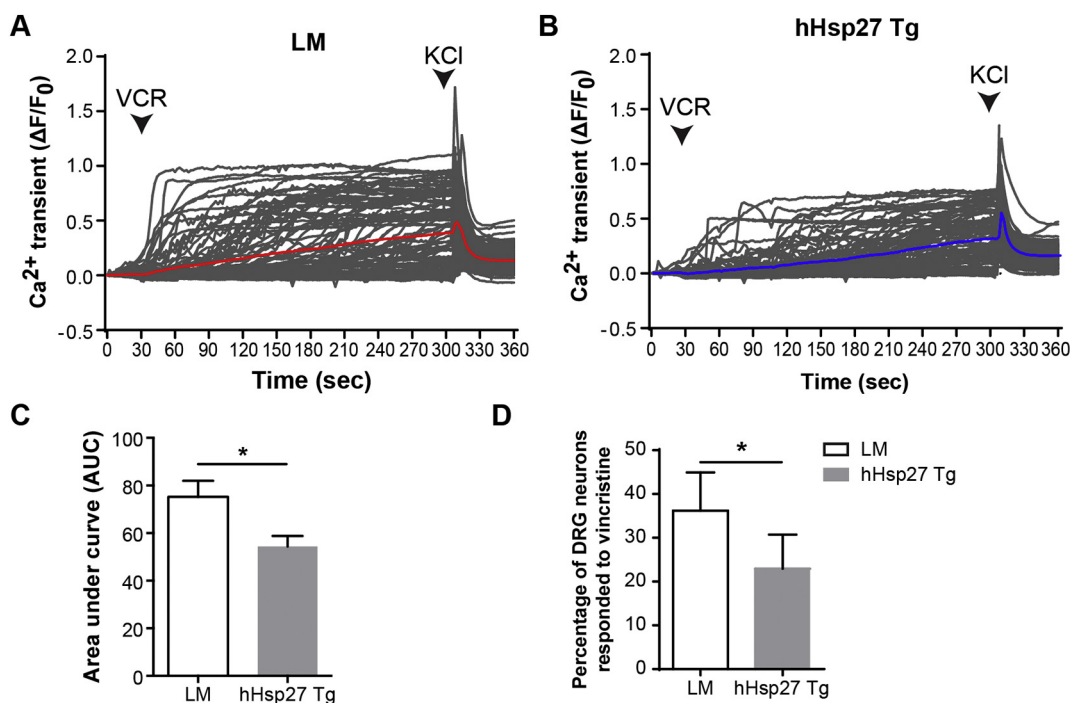


Fig. 8. hHsp27 attenuates vincristine-induced intracellular calcium influx in adult primary dorsal root ganglion neurons. (A, B) Change in fluorescence intensity ($\Delta F/F_0$) of (A) wild type LM and (B) hHsp27-expressing DRG neurons after vincristine treatment. (C) Calcium influx for each single neuron was quantified by calculating the area under the curve (AUC) of Fura-2 traces. AUC was depicted in arbitrary units which represented the total amount of calcium influx after vincristine treatment. The magnitude of calcium influx was significantly reduced in hHsp27 DRG neurons when compared with LM. Vincristine induced an increase in intracellular calcium level as shown by the area under the curve. (D) The percentage of vincristine-responding cells was markedly reduced in hHsp27-expressing neurons when compared with LM DRG neurons. Mean \pm SEM of triplicates. * P < .05, Student's *t*-test.

channel inositol trisphosphate receptor (InsP3R) and blocks ATP-evoked IP3R-mediated calcium release from the endoplasmic reticulum in human SH-SY5Y cells (Benbow et al., 2012; Pease-Raissi et al., 2017). In cultured superior cervical ganglion neurons, vinblastine treatment reduces mitochondrial membrane potential dramatically, causing mitochondrial dysfunction via the opening of the mitochondrial permeability transition pore (mPTP) (Ikegami and Koike, 2003). These studies suggest that mechanical injury-induced and chemotherapy-induced axonal degeneration is calcium-dependent. Therapeutic strategies to maintain calcium homeostasis by either blocking calcium channels or sequestering cytosolic calcium partially reverse some CIPN symptoms in rodents (Flatters and Bennett, 2004; Muthuraman et al., 2008; Siau and Bennett, 2006; Xiao et al., 2007), suggesting that strategies to simultaneously target multiple aspects of CIPN pathology, such as axonal and myelin integrity, are required.

Further studies have hypothesized that mitochondrial dysfunction is the major cause of the aberrant regulation of calcium homeostasis induced by CIPN-causing antineoplastic agents (Starobova and Vetter, 2017). For instance, in paclitaxel-treated rats, swollen and vacuolated mitochondria are observed in both unmyelinated and myelinated axons in the saphenous nerves (Flatters and Bennett, 2006). Paclitaxel induces opening of the mPTP and rapid depolarization of mitochondria (i.e., loss of mitochondrial membrane potential), which triggers calcium efflux from mitochondria into the cytosol of neurons (Mironov et al., 2005). Axonal transport of mitochondria and neurite extension are impaired after treatment with vincristine in the SK-N-SH neuronal cell line (Rovini et al., 2010). Likewise, vincristine induced mitochondrial fragmentation, disrupted axonal transport of mitochondria and caused axonal degeneration 10 h following vincristine treatment in primary DRG neurons (Barrientos et al., 2011; Berbusse et al., 2016). Restoring mitochondrial membrane potential by olesoxime application or genetic deletion of cyclophilin D (a functional component of mPTP) can overcome paclitaxel- and vincristine-induced neurite outgrowth inhibition

in vitro (Barrientos et al., 2011; Rovini et al., 2010) and partially reverses mechanical allodynia in vivo (Bordet et al., 2008; Xiao et al., 2009). This implies that reversal of mitochondrial dysfunction and restoration of aberrant calcium homeostasis could be of high therapeutic potential for preventing the development of vincristine-induced CIPN.

Vincristine induces a rapid decrease in mitochondrial membrane potential in nonneuronal cells (Groninger et al., 2002), and it is plausible that vincristine triggers opening of the mPTP, leading to aberrant efflux of mitochondrial calcium into the cytosol of DRG neurons. In the current study, we demonstrated that forced expression of hHsp27 prevents vincristine-induced mitochondrial swelling and maintains the mitochondrial membrane potential in distal nerves. Well-preserved mitochondrial integrity prevents excessive calcium release from mitochondria into the cytosol of hHsp27-overexpressing DRG neurons, and therefore prevents the activation of the caspase-3 apoptotic cascade and subsequent axonal degeneration (Ikegami and Koike, 2003). Our results support previous findings that Jurkat 2 cells overexpressing Hsp27 maintain their mitochondrial membrane potential, thereby preventing cytochrome *c* release to induce downstream caspase-3 apoptotic pathways, upon challenge with a high dose of gamma radiation (Aloy et al., 2008). Overexpression of Hsp27 protects cortical neurons from neuronal cell death following ischemic brain injury by inhibiting caspase-3 activation and cytochrome *c* release (Stetler et al., 2008). Forced expression of hHsp27 also prevents the loss of motor neurons in neonatal mice following sciatic nerve crush injury (Sharp et al., 2006). Recent studies have demonstrated that CIPN symptoms can be partially reversed by blocking cisplatin- or paclitaxel-induced neuronal apoptosis by treatment with recombinant vascular endothelial growth factor protein or CX3CL1-neutralizing antibodies, respectively (Huang et al., 2014; Vencappa et al., 2015). Taken together, our study demonstrates that forced expression of hHsp27 completely reverses vincristine-induced CIPN symptoms by targeting multiple aspects of CIPN pathology, including axonal and mitochondrial integrity as well

as calcium homeostasis. We strongly believe that the protective role of Hsp27 in CIPN will provide insight into the development of preventive and therapeutic approaches for CIPN. Further bioinformatics studies are needed to identify small molecules that activate key signaling pathways of hHsp27.

Author contributions

VC carried out the neurobehavioral assessment, in vivo electrophysiological recording, immunohistochemistry of skin and nerve biopsies, electron microscopy, TUNEL assay, Western blot analysis and calcium imaging. NPBA performed in vitro DRG culture and neurite outgrowth assay. CHEM conceived the project, designed the study and wrote the manuscript with inputs from all authors. All authors read and approved the manuscript.

Acknowledgment

This work is supported in part by General Research Fund (GRF) from The Research Grant Council of the Hong Kong Special Administrative Region Government (CityU 11100015, CityU 11100417, and CityU 11100318), and The Health and Medical Research Fund (HMRF), Food and Health Bureau, Hong Kong Special Administrative Region Government (Ref. no.: 05160126), The Innovation and Technology Fund, Innovation and Technology Commission (Ref. no.: ITS/151/17), and The CityU Applied Research Grant, City University of Hong Kong (Ref. no.: 9667149) award to Chi Ma.

Competing interests

The authors report no competing interests.

References

- Aloy, M.T., et al., 2008. Protective role of Hsp27 protein against gamma radiation-induced apoptosis and radiosensitization effects of Hsp27 gene silencing in different human tumor cells. *Int. J. Radiat. Oncol. Biol. Phys.* 70, 543–553.
- Asthana, P., et al., 2018. Pacific ciguatoxin induces excitotoxicity and neurodegeneration in the motor cortex via caspase 3 activation: implication for irreversible motor deficit. *Mol. Neurobiol.* 1–19.
- Au, N.P., et al., 2014. Probing for chemotherapy-induced peripheral neuropathy in live dorsal root ganglion neurons with atomic force microscopy. *Nanomedicine* 10, 1323–1333.
- Au, N.P., et al., 2016. Ciguatoxin reduces regenerative capacity of axotomized peripheral neurons and delays functional recovery in pre-exposed mice after peripheral nerve injury. *Sci. Rep.* 6, 26809.
- Avery, M.A., et al., 2012. WldS prevents axon degeneration through increased mitochondrial flux and enhanced mitochondrial Ca²⁺ buffering. *Curr. Biol.* 22, 596–600.
- Barrientos, S.A., et al., 2011. Axonal degeneration is mediated by the mitochondrial permeability transition pore. *J. Neurosci.* 31, 966–978.
- Benbow, J.H., et al., 2012. Inhibition of paclitaxel-induced decreases in calcium signaling. *J. Biol. Chem.* 287, 37907–37916.
- Benn, S.C., et al., 2002. Hsp27 upregulation and phosphorylation is required for injured sensory and motor neuron survival. *Neuron* 36, 45–56.
- Benndorf, R., et al., 1994. Phosphorylation and supramolecular organization of murine small heat shock protein HSP25 abolish its actin polymerization-inhibiting activity. *J. Biol. Chem.* 269, 20780–20784.
- Bennett, G.J., et al., 2011. Terminal arbor degeneration—a novel lesion produced by the antineoplastic agent paclitaxel. *Eur. J. Neurosci.* 33, 1667–1676.
- Berbusse, G.W., et al., 2016. Mitochondrial dynamics decrease prior to axon degeneration induced by vincristine and are partially rescued by overexpressed cytNmmt1. *Front. Cell. Neurosci.* 10, 179.
- Berridge, M.J., 1998. Neuronal calcium signaling. *Neuron* 21, 13–26.
- Berridge, M.J., et al., 2000. The versatility and universality of calcium signalling. *Nat. Rev. Mol. Cell Biol.* 1, 11–21.
- Boehmerle, W., et al., 2006. Paclitaxel induces calcium oscillations via an inositol 1,4,5-trisphosphate receptor and neuronal calcium sensor 1-dependent mechanism. *Proc. Natl. Acad. Sci. U. S. A.* 103, 18356–18361.
- Boehmerle, W., et al., 2014. Electrophysiological, behavioral and histological characterization of paclitaxel, cisplatin, vincristine and bortezomib-induced neuropathy in C57BL/6 mice. *Sci. Rep.* 4, 6370.
- Bordet, T., et al., 2008. Specific antinociceptive activity of cholest-4-en-3-one, oxime (TRO19622) in experimental models of painful diabetic and chemotherapy-induced neuropathy. *J. Pharmacol. Exp. Ther.* 326, 623–632.
- Boyette-Davis, J., Dougherty, P.M., 2011. Protection against oxaliplatin-induced mechanical hyperalgesia and intraepidermal nerve fiber loss by minocycline. *Exp. Neurol.* 229, 353–357.
- Boyette-Davis, J., et al., 2011. Intraepidermal nerve fiber loss corresponds to the development of taxol-induced hyperalgesia and can be prevented by treatment with minocycline. *Pain* 152, 308–313.
- Brini, M., et al., 2014. Neuronal calcium signaling: function and dysfunction. *Cell. Mol. Life Sci.* 71, 2787–2814.
- Canta, A., et al., 2015. Mitochondrial dysfunction in chemotherapy-induced peripheral neuropathy (CIPN). *Toxicol. Appl. Pharmacol.* 283, 198–223.
- Caroni, P., 1997. Overexpression of growth-associated proteins in the neurons of adult transgenic mice. *J. Neurosci. Methods* 71, 3–9.
- Carozzi, V.A., et al., 2015. Chemotherapy-induced peripheral neuropathy: what do we know about mechanisms? *Neurosci. Lett.* 596, 90–107.
- Cashman, C.R., Hoke, A., 2015. Mechanisms of distal axonal degeneration in peripheral neuropathies. *Neurosci. Lett.* 596, 33–50.
- Chan, S.Y., et al., 1980. Block of axoplasmic transport in vitro by vinca alkaloids. *J. Neurobiol.* 11, 251–264.
- Chaudhry, V., et al., 1994. Peripheral neuropathy from taxol and cisplatin combination chemotherapy: clinical and electrophysiological studies. *Ann. Neurol.* 35, 304–311.
- Chaudhuri, S., Smith, P.G., 2008. Cyclic strain-induced HSP27 phosphorylation modulates actin filaments in airway smooth muscle cells. *Am. J. Respir. Cell Mol. Biol.* 39, 270–278.
- Chine, V.B., et al., 2019. Targeting axon integrity to prevent chemotherapy-induced peripheral neuropathy. *Mol. Neurobiol.* 56, 3244–3259.
- Cho, Y., et al., 2013. Injury-induced HDAC5 nuclear export is essential for axon regeneration. *Cell* 155, 894–908.
- Coleman, M.P., Freeman, M.R., 2010. Wallerian degeneration, wld(s), and nmnats. *Annu. Rev. Neurosci.* 33, 245–267.
- Concannon, C.G., et al., 2003. On the role of Hsp27 in regulating apoptosis. *Apoptosis* 8, 61–70.
- Costigan, M., et al., 1998. Heat shock protein 27: developmental regulation and expression after peripheral nerve injury. *J. Neurosci.* 18, 5891–5900.
- Costigan, M., et al., 2002. Replicate high-density rat genome oligonucleotide microarrays reveal hundreds of regulated genes in the dorsal root ganglion after peripheral nerve injury. *BMC Neurosci.* 3, 16.
- Cunha, T.M., et al., 2004. An electronic pressure-meter nociception paw test for mice. *Braz. J. Med. Biol. Res.* 37, 401–407.
- Dasari, S., Tchounwou, P.B., 2014. Cisplatin in cancer therapy: molecular mechanisms of action. *Eur. J. Pharmacol.* 740, 364–378.
- Deangelis, L.M., et al., 1991. Evolution of neuropathy and myopathy during intensive vincristine/corticosteroid chemotherapy for non-hodgkin's lymphoma. *Cancer* 67, 2241–2246.
- Decosterd, I., Woolf, C.J., 2000. Spared nerve injury: an animal model of persistent peripheral neuropathic pain. *Pain* 87, 149–158.
- Deuis, J.R., et al., 2013. An animal model of oxaliplatin-induced cold allodynia reveals a crucial role for Nav1.6 in peripheral pain pathways. *Pain* 154, 1749–1757.
- Flatters, S.J., Bennett, G.J., 2004. Ethosuximide reverses paclitaxel- and vincristine-induced painful peripheral neuropathy. *Pain* 109, 150–161.
- Flatters, S.J., Bennett, G.J., 2006. Studies of peripheral sensory nerves in paclitaxel-induced painful peripheral neuropathy: evidence for mitochondrial dysfunction. *Pain* 122, 245–257.
- Fletcher, E.V., et al., 2017. Reduced sensory synaptic excitation impairs motor neuron function via Kv2.1 in spinal muscular atrophy. *Nat. Neurosci.* 20, 905.
- Freilich, R.J., et al., 1996. Motor neuropathy due to docetaxel and paclitaxel. *Neurology* 47, 115–118.
- Fukuda, Y., et al., 2017. A mechanistic understanding of axon degeneration in chemotherapy-induced peripheral neuropathy. *Front. Neurosci.* 11, 481.
- Geis, C., et al., 2011. Lauroamide has protective disease modifying properties in experimental vincristine neuropathy. *Neuropharmacology* 61, 600–607.
- Geisler, S., et al., 2016. Prevention of vincristine-induced peripheral neuropathy by genetic deletion of SARM1 in mice. *Brain* 139, 3092–3108.
- Gleichmann, M., Mattson, M.P., 2011. Neuronal calcium homeostasis and dysregulation. *Antioxid. Redox Signal.* 14, 1261–1273.
- Gornstein, E., Schwarz, T.L., 2014. The paradox of paclitaxel neurotoxicity: mechanisms and unanswered questions. *Neuropharmacology* 76 Pt A, 175–183.
- Gottschalk, P., et al., 1968. Vinca alkaloid neuropathy: nerve biopsy studies in rats and in man. *Neurology* 18, 875.
- Griffin, R.S., et al., 2007. Complement induction in spinal cord microglia results in anaphylatoxin C5a-mediated pain hypersensitivity. *J. Neurosci.* 27, 8699–8708.
- Groninger, E., et al., 2002. Vincristine induced apoptosis in acute lymphoblastic leukaemia cells: a mitochondrial controlled pathway regulated by reactive oxygen species? *Int. J. Oncol.* 21, 1339–1345.
- Haim, N., et al., 1994. Full dose vincristine (without 2-mg dose limit) in the treatment of lymphomas. *Cancer* 73, 2515–2519.
- Han, Y., Smith, M.T., 2013. Pathobiology of cancer chemotherapy-induced peripheral neuropathy (CIPN). *Front. Pharmacol.* 4, 156.
- Hershman, D.L., et al., 2014. Prevention and management of chemotherapy-induced peripheral neuropathy in survivors of adult cancers: American Society of Clinical Oncology clinical practice guideline. *J. Clin. Oncol.* 32, 1941–1967.
- Hill, R.Z., et al., 2018. S1PR3 mediates itch and pain via distinct TRP channel-dependent pathways. *J. Neurosci.* 38, 7833–7843.
- Ho, Y.M., et al., 2014. A lysosome-specific two-photon phosphorescent binuclear cyclo-metalated platinum(II) probe for in vivo imaging of live neurons. *Chem. Commun. (Camb.)* 50, 4161–4163.
- Huang, Z.Z., et al., 2014. CX3CL1-mediated macrophage activation contributed to

- paclitaxel-induced DRG neuronal apoptosis and painful peripheral neuropathy. *Brain Behav. Immun.* 40, 155–165.
- Huehnchen, P., et al., 2013. Assessment of paclitaxel induced sensory polyneuropathy with "catwalk" automated gait analysis in mice. *PLoS One* 8, e76772.
- Huot, J., et al., 1996. HSP27 phosphorylation-mediated resistance against actin fragmentation and cell death induced by oxidative stress. *Cancer Res.* 56, 273–279.
- Ikegami, K., Koike, T., 2003. Non-apoptotic neurite degeneration in apoptotic neuronal death: pivotal role of mitochondrial function in neurites. *Neuroscience* 122, 617–626.
- Jaggi, A.S., Singh, N., 2012. Mechanisms in cancer-chemotherapeutic drugs-induced peripheral neuropathy. *Toxicology* 291, 1–9.
- Jordan, M.A., Wilson, L., 2004. Microtubules as a target for anticancer drugs. *Nat. Rev. Cancer* 4, 253–265.
- Jordan, M.A., et al., 1991. Mechanism of inhibition of cell proliferation by Vinca alkaloids. *Cancer Res.* 51, 2212–2222.
- Kaur, G., et al., 2010. Exploring the potential effect of Ocimum sanctum in vincristine-induced neuropathic pain in rats. *J. Brachial Plex. Peripher. Nerve Inj.* 5, 3.
- Kidd, J.F., et al., 2002. Paclitaxel affects cytosolic calcium signals by opening the mitochondrial permeability transition pore. *J. Biol. Chem.* 277, 6504–6510.
- Konings, P.N., et al., 1994. Reversal by NGF of cytostatic drug-induced reduction of neurite outgrowth in rat dorsal root ganglia in vitro. *Brain Res.* 640, 195–204.
- Korngut, L., et al., 2012. Overexpression of human HSP27 protects sensory neurons from diabetes. *Neurobiol. Dis.* 47, 436–443.
- Kroigard, T., et al., 2014. Characterization and diagnostic evaluation of chronic polyneuropathies induced by oxaliplatin and docetaxel comparing skin biopsy to quantitative sensory testing and nerve conduction studies. *Eur. J. Neurol.* 21, 623–629.
- Lauria, G., et al., 2005. Intraepidermal nerve fiber density in rat foot pad: neuropathologic-neurophysiologic correlation. *J. Peripher. Nerv. Syst.* 10, 202–208.
- Lavoie Smith, E.M., et al., 2015. Patterns and severity of vincristine-induced peripheral neuropathy in children with acute lymphoblastic leukemia. *J. Peripher. Nerv. Syst.* 20, 37–46.
- Lavoie, J.N., et al., 1993. Induction of Chinese hamster HSP27 gene expression in mouse cells confers resistance to heat shock. HSP27 stabilization of the microfilament organization. *J. Biol. Chem.* 268, 3420–3429.
- Li, Y., et al., 2017. Dorsal root ganglion neurons become hyperexcitable and increase expression of voltage-gated T-type calcium channels (Cav3.2) in paclitaxel-induced peripheral neuropathy. *Pain* 158, 417–429.
- Liu, C.N., et al., 2017. A novel endpoint for the assessment of chemotherapy-induced peripheral neuropathy in rodents: biomechanical properties of peripheral nerve. *J. Appl. Toxicol.* 38 (2), 193–200.
- Ma, C.H., et al., 2011a. The BMP coreceptor RGMb promotes while the endogenous BMP antagonist noggin reduces neurite outgrowth and peripheral nerve regeneration by modulating BMP signaling. *J. Neurosci.* 31, 18391–18400.
- Ma, C.H., et al., 2011b. Accelerating axonal growth promotes motor recovery after peripheral nerve injury in mice. *J. Clin. Invest.* 121, 4332–4347.
- Martinov, T., et al., 2013. Measuring changes in tactile sensitivity in the hind paw of mice using an electronic von Frey apparatus. *J. Vis. Exp.* 19 (82), e51212.
- Meijer, C., et al., 1999. Cisplatin-induced DNA-platinatin in experimental dorsal root ganglia neuropathy. *Neurotoxicology* 20, 883–887.
- Meyer, O.A., et al., 1979. A method for the routine assessment of fore- and hindlimb grip strength of rats and mice. *Neurobehav. Toxicol.* 1, 233–236.
- Mironov, S.L., et al., 2005. [Ca²⁺]i signaling between mitochondria and endoplasmic reticulum in neurons is regulated by microtubules. From mitochondrial permeability transition pore to Ca²⁺-induced Ca²⁺ release. *J. Biol. Chem.* 280, 715–721.
- Muchowski, P.J., 2002. Protein misfolding, amyloid formation, and neurodegeneration: a critical role for molecular chaperones? *Neuron* 35, 9–12.
- Muthuraman, A., et al., 2008. Ameliorative effects of amiloride and pralidoxime in chronic constriction injury and vincristine induced painful neuropathy in rats. *Eur. J. Pharmacol.* 587, 104–111.
- Painter, M.W., et al., 2014. Diminished Schwann cell repair responses underlie age-associated impaired axonal regeneration. *Neuron* 83, 331–343.
- Pan, Y.A., et al., 2003. Effects of neurotoxic and neuroprotective agents on peripheral nerve regeneration assayed by time-lapse imaging in vivo. *J. Neurosci.* 23, 11479–11488.
- Park, S.B., et al., 2013. Chemotherapy-induced peripheral neurotoxicity: a critical analysis. *CA Cancer J. Clin.* 63, 419–437.
- Pease-Raiissi, S.E., et al., 2017. Paclitaxel reduces axonal Bclw to initiate IP 3 R1-dependent axon degeneration. *Neuron* 96, 373–386 e6.
- Peltier, A.C., Russell, J.W., 2002. Recent advances in drug-induced neuropathies. *Curr. Opin. Neurol.* 15, 633–638.
- Periquet, M.I., et al., 1999. Painful sensory neuropathy: prospective evaluation using skin biopsy. *Neurology* 53, 1641–1647.
- Pichon, S., et al., 2004. Control of actin dynamics by p38 MAP kinase – Hsp27 distribution in the lamellipodium of smooth muscle cells. *J. Cell Sci.* 117, 2569–2577.
- Quasthoff, S., Hartung, H.P., 2002. Chemotherapy-induced peripheral neuropathy. *J. Neurol.* 249, 9–17.
- Rosenthal, S., Kaufman, S., 1974. Vincristine neurotoxicity. *Ann. Intern. Med.* 80, 733–737.
- Rovini, A., et al., 2010. Olesoxime prevents microtubule-targeting drug neurotoxicity: selective preservation of EB comets in differentiated neuronal cells. *Biochem. Pharmacol.* 80, 884–894.
- Seretny, M., et al., 2014. Incidence, prevalence, and predictors of chemotherapy-induced peripheral neuropathy: a systematic review and meta-analysis. *Pain* 155, 2461–2470.
- Sharp, P., et al., 2006. Heat shock protein 27 rescues motor neurons following nerve injury and preserves muscle function. *Exp. Neurol.* 198, 511–518.
- Siau, C., Bennett, G.J., 2006. Dysregulation of cellular calcium homeostasis in chemotheraphy-evoked painful peripheral neuropathy. *Anesth. Analg.* 102, 1485–1490.
- Siau, C., et al., 2006. Paclitaxel- and vincristine-evoked painful peripheral neuropathies: loss of epidermal innervation and activation of Langerhans cells. *Exp. Neurol.* 201, 507–514.
- Snutch, T.P., 2005. Targeting chronic and neuropathic pain: the N-type calcium channel comes of age. *NeuroRx.* 2, 662–670.
- Staff, N.P., et al., 2017. Chemotherapy-induced peripheral neuropathy: a current review. *Ann. Neurol.* 81, 772–781.
- Starobova, H., Vetter, I., 2017. Pathophysiology of chemotherapy-induced peripheral neuropathy. *Front. Mol. Neurosci.* 10, 174.
- Stetler, R.A., et al., 2008. Hsp27 protects against ischemic brain injury via attenuation of a novel stress-response cascade upstream of mitochondrial cell death signaling. *J. Neurosci.* 28, 13038–13055.
- Van Helleputte, L., et al., 2018. Inhibition of histone deacetylase 6 (HDAC6) protects against vincristine-induced peripheral neuropathies and inhibits tumor growth. *Neurobiol. Dis.* 111, 59–69.
- Vanegas, H., Schaible, H., 2000. Effects of antagonists to high-threshold calcium channels upon spinal mechanisms of pain, hyperalgesia and allodynia. *Pain* 85, 9–18.
- Vargas, M.E., et al., 2015. Live imaging of calcium dynamics during axon degeneration reveals two functionally distinct phases of calcium influx. *J. Neurosci.* 35, 15026–15038.
- Vencappa, S., et al., 2015. Cisplatin induced sensory neuropathy is prevented by vascular endothelial growth factor-A. *Am. J. Transl. Res.* 7, 1032–1044.
- Vink, S., Alewood, P.F., 2012. Targeting voltage-gated calcium channels: developments in peptide and small-molecule inhibitors for the treatment of neuropathic pain. *Br. J. Pharmacol.* 167, 970–989.
- Vuorinen, V.S., Roytta, M., 1990. Taxol-induced neuropathy after nerve crush: long-term effects on regenerating axons. *Acta Neuropathol.* 79, 663–671.
- Wang, M.S., et al., 2000. Pathogenesis of axonal degeneration: parallels between Wallerian degeneration and vincristine neuropathy. *J. Neuropathol. Exp. Neurol.* 59, 599–606.
- Wang, M.S., et al., 2002. WldS mice are resistant to paclitaxel (taxol) neuropathy. *Ann. Neurol.* 52, 442–447.
- Wang, M.S., et al., 2004. Calpain inhibition protects against Taxol-induced sensory neuropathy. *Brain* 127, 671–679.
- Wilhelmsen, M.M., et al., 2006. Small heat shock protein HspB8: its distribution in Alzheimer's disease brains and its inhibition of amyloid-beta protein aggregation and cerebrovascular amyloid-beta toxicity. *Acta Neuropathol.* 111, 139–149.
- Windebank, A.J., Grisold, W., 2008. Chemotherapy-induced neuropathy. *J. Peripher. Nerv. Syst.* 13, 27–46.
- Xiao, W.H., Bennett, G.J., 2008. Chemotherapy-evoked neuropathic pain: abnormal spontaneous discharge in A-fiber and C-fiber primary afferent neurons and its suppression by acetyl-L-carnitine. *Pain* 135, 262–270.
- Xiao, W., et al., 2007. Chemotherapy-evoked painful peripheral neuropathy: analgesic effects of gabapentin and effects on expression of the alpha-2-delta type-1 calcium channel subunit. *Neuroscience* 144, 714–720.
- Xiao, W.H., et al., 2009. Olesoxime (cholest-4-en-3-one, oxime): analgesic and neuroprotective effects in a rat model of painful peripheral neuropathy produced by the chemotherapeutic agent, paclitaxel. *Pain* 147, 202–209.
- Zamponi, G.W., et al., 2009. Role of voltage-gated calcium channels in ascending pain pathways. *Brain Res. Rev.* 60, 84–89.
- Zhou, B., et al., 2016. Facilitation of axon regeneration by enhancing mitochondrial transport and rescuing energy deficits. *J. Cell Biol.* 214, 103–119.